

Quantifying the Effects of Contact Tracing, Testing, and Containment

Lars Lorch¹, Heiner Kremer², William Trouleau³, Stratis Tsirtsis⁴, Aron Szanto⁵,
Bernhard Schölkopf^{2,1}, Manuel Gomez-Rodriguez⁴

¹ETH Zürich, llorch@student.ethz.ch

²Max Planck Institute for Intelligent Systems, {heiner.kremer,bs}@tuebingen.mpg.de

³École Polytechnique Fédérale de Lausanne, william.trouleau@epfl.ch

⁴Max Planck Institute for Software Systems, {stsirtsis,manuelgr}@mpi-sws.org

⁵Zerobase Foundation, aron@zerobase.io

December 22, 2024

Abstract

Contact tracing has the potential to help identify, characterize, and predict disease-spreading human interactions at an unprecedented resolution. However, to realize this potential, we need to utilize data-driven epidemic models that can operate at a high spatiotemporal resolution and make use of and benefit from contact tracing data of individuals. Such data-driven models are currently missing, and in this work we initiate their development using the framework of temporal point processes. Using an efficient sampling algorithm, we can use our model to quantify the effects that different testing and tracing strategies, social distancing measures, and business restrictions may have on the course of the disease. Building on this algorithm, we use Bayesian optimization to estimate the transmission rate due to infectious individuals at the sites they visit and at their households as well as the mobility reduction due to social distancing from longitudinal case data. Simulations using real COVID-19 case data and mobility patterns from several cities and regions in Germany and Switzerland with a wide range of infection levels until today demonstrate that our model may allow individuals and policy makers to make more effective decisions.

1 Introduction

The novel coronavirus disease COVID-19 has spread from Wuhan to the rest of the world in a matter of months [1, 2]. Until vaccines become widely available, policymakers need to resort to testing and isolation, contact tracing, physical distancing, and other containment measures to prevent its spread. In this context, there have been burgeoning efforts to introduce digital contact tracing systems for automated and fine-grained monitoring of individual contacts. Among them, we can distinguish between location-based systems, such as GPS or QR code check-ins [3, 4] and proximity-based systems, such as Bluetooth [5–7]. Here, we argue that automated and fine-grained monitoring of individual contacts may allow for:

- I. **More accurate predictions.** New data sources may allow us to predict the spread of COVID-19 at an unprecedented spatiotemporal resolution. This includes when and where new individual infections may happen and how likely these events are to occur.
- II. **More effective containment and mitigation.** Tracing systems may help us design more effective strategies to slow down or even prevent the spread of COVID-19, thus allowing authorities to gradually lift the most restrictive measures with more precision and confidence.

III. Data-driven insights into disease parameters. Accurate contact tracing may yield insights into the relative importance of different modalities of disease transmission and allow inference of the unknown parameters of the transmission and course of COVID-19.

However, to realize the above mentioned capabilities, we need to utilize data-driven models and algorithms that can operate at a high spatiotemporal resolution and make use of contact tracing data of individuals. Unfortunately, such data-driven models and algorithms are currently missing. Most of the classical epidemiological literature [8–12] has primarily focused on developing models for general population dynamics rather than the infectious state of any given individual in the population. More recently, there has been research on modeling individual dynamics of epidemics [13–17], yet this work typically resorts to mean-field theory and thus does not characterize the dynamic infectious state of each individual over time. Finally, in the context of the current COVID-19 outbreak, there has been a flurry of work on agent-based epidemic models [18–31]. However, these models make simplistic assumptions about individual mobility patterns and do not use COVID-19 case data to estimate their model parameters. As a consequence, they are unable to accurately characterize the fine-grained effects of testing, contact tracing, and containment measures on individuals living in geographically diverse regions.

In this work, we develop a flexible modeling framework that is specifically designed to make use of contact tracing data and make fine-grained spatiotemporal predictions about individual disease spread. Our model uses marked temporal point processes [32] to represent events when individuals ...

- ... are exposed, asymptomatic, presymptomatic, symptomatic, hospitalized, recovered, or dead (*Epidemiology*).
- ... check in at different points of interest, where they get in contact with and possibly infect each other (*Mobility*).
- ... are affected by measures such as social distancing and quarantines, or points of interest implement hygienic and capacity-limiting policies (*Containment measures*).
- ... get tested by health authorities or receive the outcome of a test (*Testing*).
- ... who were in contact with positively tested individuals are tracked down (*Contact tracing*).

Within this paradigm, our modeling framework is fully defined by way of a set of conditional intensity functions, or hazard functions. To realistically model the exposure of individuals at sites, our framework introduces a new intensity function that is able to characterize the influence that mobility patterns as well as containment measures have on the risk that each infected individual poses to their community. Our framework is agnostic to the particular model of mobility patterns and can directly use almost any form of real mobility data when available, including contact tracing data.

In addition, we design an efficient sampling algorithm for our model, which allows us to simulate the spread of COVID-19 under a variety of interventions and what-if scenarios using Monte Carlo roll-outs. Moreover, building on our sampling algorithm, we use Bayesian optimization [33–35] to estimate the transmission rate due to infectious individuals at the sites they visit, in their households, as well as the mobility reduction due to social distancing from longitudinal case data. Finally, we showcase our modeling framework using real COVID-19 case data and mobility patterns from several cities and regions in Germany and Switzerland with a wide range of infection levels until today. Our results show that our model can be used to estimate the effect of testing, contact tracing, and containment measures at an unprecedented spatiotemporal resolution and may ultimately allow individuals and policy makers to make more effective decisions. To enable further research in this area, we release an open-source implementation of our framework [36].

2 A Spatiotemporal Model of Epidemics

Given a set of individuals \mathcal{V} , we track the current state of each single individual $i \in \mathcal{V}$ using a collection of state variables, which determine their mobility pattern, epidemiological condition, and degree of testing and contact tracing, under different social distancing measures and business restrictions. We use stochastic

Table 1: Epidemiological state variables

State	Description	Infected	Contagious	Symptoms
$S_i(t)$	is susceptible	-	-	-
$E_i(t)$	is exposed	✓	-	-
$I_i^a(t)$	is asymptomatic, has mild course of disease	✓	✓	-
$I_i^p(t)$	is pre-symptomatic, progresses to $I_i^s(t)$ later on	✓	✓	-
$I_i^s(t)$	is symptomatic	✓	✓	✓
$H_i(t)$	is hospitalized	✓	✓	✓
$R_i(t)$	is resistant and recovered	-	-	-
$D_i(t)$	has died	-	-	-

differential equations (SDEs) with jumps to realistically model *(i)* the stochastic nature of mobility patterns and infection events, *(ii)* events in continuous time, i.e. *not* in aggregate over days, and *(iii)* discrete state transitions — an individual either does *or* does not get infected, visit a site, or is selected for quarantine. To ease the exposition, we describe different types of state variables separately.

2.1 Mobility

Let \mathcal{S} be the set of *sites* individuals can visit. For each individual i , let the indicator $P_{i,k}(t) = 1$ if the individual is at site $k \in \mathcal{S}$ at time t and $P_{i,k}(t) = 0$ otherwise. We characterize the value of the states $P_{i,k}(t) = 1$ using the following SDE with jumps:

$$dP_{i,k}(t) = dU_{i,k}(t) - dV_{i,k}(t) \quad (1)$$

where $U_{i,k}(t)$ and $V_{i,k}(t)$ are counting processes indicating when individual i arrives at and leaves site $k \in \mathcal{S}$, respectively. Moreover, we define their intensities as follows:

$$\begin{aligned} \mathbb{E}[dU_{i,k}(t)|\mathcal{H}(t)] &= \lambda_{i,k}(t) \prod_{l \in \mathcal{S}} (1 - P_{i,l}(t)) dt \\ \mathbb{E}[dV_{i,k}(t)|\mathcal{H}(t)] &= U_{i,k}(t) v_k dt \end{aligned} \quad (2)$$

where $\lambda_{i,k}(t)$ is the rate at which the individual visits site k and $1/v_k$ is the average duration of a visit to site k , which can be modeled to depend on the individuals age $a(i) \in \mathcal{A}$ of age groups \mathcal{A} . From now on and above, $\mathcal{H}(t)$ denotes the history of arrivals of the corresponding counting processes. This model of mobility can be substituted by almost any form of real mobility data as long as $P_{i,k}(t)$ is defined, which is the case for both location and proximity-based contact tracing systems. Here, for proximity-based mobility data, we can define a site $k_{i,j}$ for each pairwise interaction between individuals i and j .

2.2 Epidemiology

We build on recent variations of the Susceptible-Exposed-Infected-Resistant (SEIR) compartment models, which have been introduced in the context of COVID-19 modeling [22, 25]. More specifically, we define the epidemiological condition of each individual $i \in \mathcal{V}$ using the indicator state variables $S_i(t)$, $E_i(t)$, $I_i^a(t)$, $I_i^p(t)$, $I_i^s(t)$, $H_i(t)$, $R_i(t)$, $D_i(t) \in \{0, 1\}$, whose meaning is specified in Table 1. Then, we characterize their values

and state transitions using the following SDEs with jumps:

$$\begin{aligned}
dS_i(t) &= -S_i(t)dN_i(t) \\
dE_i(t) &= dN_i(t) - dM_i(t) \\
dI_i^a(t) &= a_i dM_i(t) - dR_i^a(t) \\
dI_i^p(t) &= (1 - a_i) dM_i(t) - dW_i(t) \\
dI_i^s(t) &= dW_i(t) - (1 - b_i) dR_i^s(t) - b_i dZ_i(t) \\
dR_i(t) &= a_i dR_i^a(t) + (1 - a_i) dR_i^s(t) \\
dH_i(t) &= h_i I_i^s(t) dY_i(t) - (1 - b_i) H_i(t) dR_i^s(t) - b_i H_i(t) dZ_i(t) \\
dD_i(t) &= b_i dZ_i(t)
\end{aligned} \tag{3}$$

where $a_i \in \{0, 1\} \sim \text{Bernoulli}(\alpha_a)$ indicates whether an infected individual i is asymptomatic, $h_i \in \{0, 1\} \sim \text{Bernoulli}(\alpha_h)$ indicates whether a symptomatic individual i eventually requires hospitalization, and $b_i \in \{0, 1\} \sim \text{Bernoulli}(\alpha_b)$ indicates whether a symptomatic individual eventually dies. The counting processes $N_i(t)$, $M_i(t)$, $R_i^a(t)$, $R_i^s(t)$, $W_i(t)$, $Y_i(t)$, and $Z_i(t)$ model the state transitions of individual i from susceptible to exposed ($N_i(t)$), from exposed to infected ($M_i(t)$), from presymptomatic infected to symptomatic infected ($W_i(t)$), from asymptomatic infected to resistant ($R_i^a(t)$), from symptomatic infected to resistant ($R_i^s(t)$), from symptomatic infected to hospitalized ($Y_i(t)$), and from symptomatic infected to dead ($Z_i(t)$).

At the core of our modeling framework, we define the conditional intensity function $\lambda_i^*(t)$ of the exposure counting process $N_i(t)$ as

$$\lambda_i^*(t) = \sum_{k \in \mathcal{S}} \beta_k P_{i,k}(t) \sum_{j \in \mathcal{V} \setminus \{i\}} \int_{t-\delta}^t K_{j,k}(\tau) e^{-\gamma(t-\tau)} d\tau \tag{4}$$

where

$$K_{j,k}(\tau) = (I_j^s(\tau) + I_j^p(\tau) + \mu I_j^a(\tau)) P_{j,k}(\tau)$$

and $\mathbb{E}[dN_i(t)|\mathcal{H}(t)] = \lambda_i^*(t) dt$. In the above, we have that

- (i) $\beta_k \geq 0$ is the transmission rate due to presymptomatic and symptomatic individuals at site k .¹
- (ii) $\mu \in [0, 1]$ is the relative transmission rate of asymptomatic compared to (pre-)symptomatic individuals.
- (iii) $\int_{t-\delta}^t K_{j,k}(\tau) e^{-\gamma(t-\tau)} d\tau$ accounts for environmental transmission, *i.e.*, it accounts for the fact that the virus may survive for some period of time on surfaces or in the air after an infected individual has left a site [37].

Intuitively, the exposure intensity in Eq. 4 models that a given individual's instantaneous rate of exposure increases by a constant site-specific transmission rate β_k when being in contact with another infectious individual, in addition to capturing environmental transmission. Note that the exposure rate of each individual i only depends on the individual's contacts, not the contact of others. Infections within households can be characterized straightforwardly by adding an additional additive rate $\lambda_{\mathcal{H}(i)}(t)$ with transmission rate ξ to the intensity $\lambda_i^*(t)$. Refer to Appendix A for more details.

We define the remaining time-to-event distributions of the disease-specific counting processes $M_i(t)$, $R_i^a(t)$, $R_i^s(t)$, $W_i(t)$, $Y_i(t)$, and $Z_i(t)$, which do not depend on the mobility model, following the recent literature on COVID-19, as described in Appendix B and Table 2.

2.3 Containment measures

We can characterize a variety of containment measures at high spatiotemporal resolution. These may range from less restrictive (*e.g.*, isolating individuals who have tested positive) to more restrictive (*e.g.*, implementing

¹ Depending on the availability of labeled and unlabeled data, one may consider different settings, such as all sites sharing the same parameter β or sites of the same category c sharing β_c .

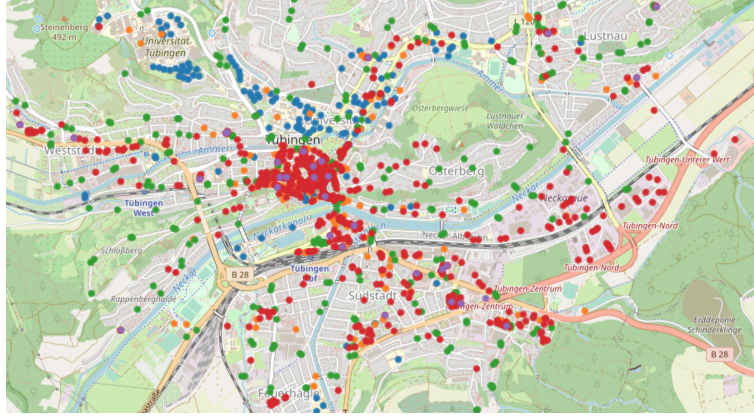


Figure 1: **Spatial distribution of site locations in the mobility model of Tübingen, Germany.** Circles depict schools, universities and research institutes (blue), social places (orange), bus stops (green), workplaces (red), and supermarkets (purple).

a state of “lockdown” for the entire population via curfews). More specifically, the effect of social distancing and quarantine can be faithfully characterized by reducing the rates $\lambda_{i,k}(t)$ at which individuals visit sites in the mobility model by a fraction p . The effect of business restrictions can be characterized by reducing (e.g., hygienic measures) or setting to zero (e.g., closures) the transmission rates β_k of the sites individuals visits. In both cases, the measures lead to a reduction of the conditional intensities $\lambda_i^*(t)$ of the exposure counting processes $N_i(t)$, possibly dynamically.

2.4 Testing

Our model maintains a queue Q_{test} of individuals to be tested. Over time, individuals are added to the queue according to a testing policy $\pi_{\text{test}}(t)$, e.g., testing only symptomatic or vulnerable people. Individuals from the queue are tested at an arbitrary rate $\lambda_{\text{test}}(t)$, and every time an individual is tested, the outcome of the test is only known after a reporting delay Δ_{test} .

More formally, let $T(t)$ record the number of known test outcomes by time t and, for each individual $i \in \mathcal{V}$, let $T_i^+(t)$ and $T_i^-(t)$ be the number of times the individual has been tested positive and negative, respectively, by time t . Then, we can characterize the counting processes $T_i^+(t)$ and $T_i^-(t)$ using the following SDEs with jumps:

$$\begin{aligned} dT_i^+(t) &= [E_i(t) + I_i^a(t) + I_i^p(t) + I_i^s(t)] d_i(t) dT(t + \Delta_{\text{test}}) \\ dT_i^-(t) &= [S_i(t) + R_i(t)] d_i(t) dT(t + \Delta_{\text{test}}) \end{aligned} \quad (5)$$

where $\mathbb{E}[dT(t)|\mathcal{H}(t)] = \lambda_{\text{test}}(t) dt$ and $d_i(t) \in \{0, 1\} \sim \pi_{\text{test}}(t)$ indicates whether an individual i is tested at time t according to the policy.

2.5 Contact tracing

When an individual i is tested positive, a subset of individuals previously in contact with i could be isolated or advised to seek testing. Under our model, a location-based contact tracing system records the times when an individual i checks in at different sites $k \in \mathcal{S}$, i.e., it observes $P_{i,k}(t)$. Therefore, it can identify the set of individuals $\mathcal{C}_{[t_0, t_f]}(i)$ who had contact with individual i during a time window $[t_0, t_f]$ at any possible site and also account for environmental transmissions. In contrast, a proximity-based contact tracing system only records the times when a pair of individuals i and j have met, i.e., have been physically close to each other, during a time window $[t_0, t_f]$. For simplicity, we overload notation and define

$P_{i,j}(t) := \sum_{k \in S} P_{i,k}(t)P_{j,k}(t) \in \{0, 1\}$ as the indicator of contact between individuals i and j . Observing $P_{i,j}(t)$, the authority can again identify the set of individuals $\mathcal{C}_{[t_0, t_f]}(i)$ who had contact with individual i during a time window $[t_0, t_f]$, however, it cannot account for environmental transmissions. To overcome this limitation, the authority could resort to data from proximity-based contact tracing systems if Bluetooth beacons are in place [38].

Once a contact tracing system has identified the contacts $\mathcal{C}_{[t_0, t_f]}(i)$ of individual i , different contact tracing policies can be implemented in various contexts. Amongst numerous strategies, we consider the possibility of allocating tests based on the empirical exposure probability of contacts of an infectious person in this work, which can be straightforwardly estimated using our framework. Refer to Appendices C and D for details.

3 Simulation and Parameter Estimation

3.1 Sampling algorithm

Given a fixed set of general individual mobility patterns $P_{i,k}(t)$ and initial conditions $S_i(0), E_i(0), \dots \forall i \in \mathcal{V}$, we develop a sampling algorithm that simulates the state of each individual in the population over a time window of interest $[0, T]$, potentially under social distancing measures, business restrictions, and a testing and tracing strategy. The challenge here is that once individual i becomes infectious, their state changes to one of $I_i^a(t) = 1$ or $I_i^p(t) = 1$, thereby changing the intensities λ_j^* of the exposure counting processes $Y_j(t)$ of other individuals j who have contact with i in the future. That means, previous timings sampled for Y_j might become invalid as the intensities of the counting processes change. As a result, sound simulations have to apply the principles of superposition and thinning [32, 39] to generate valid samples of $Y_i(t)$ as infectious states change over time. Refer to Appendix E for a detailed description of our algorithm.

3.2 Parameter estimation using Bayesian optimization

We use Bayesian optimization (BO) [35] to jointly estimate a set of exposure-related parameters θ that best fit the longitudinal case data and were not specified from the literature. BO techniques provide sample-efficient global optimization [33, 34], making them suitable for the computationally intensive simulations used in our model. BO has been previously used for parameter estimation in expensive-to-evaluate models [40].

Bayesian optimization. In BO, a probabilistic *surrogate model* tracks the posterior p of the observed black-box function f given a set of observed noisy evaluations \mathcal{D} . As commonly done, we use a Gaussian process (GP). New function evaluations are treated as observations used to update the posterior of the objective. An *acquisition function* defined over the surrogate model guides the exploration-vs.-exploitation strategy. At each iteration of the procedure, the acquisition function is cheaply optimized to determine the next point of function evaluation [33, 41]. The function guides the search for an optimum, typically defined such that high acquisition corresponds to high potential improvement of the objective.

Black-box simulator. We define the black-box functions observed from our simulator as the *mean number of positive cases at time t*

$$g_t(\theta) = \mathbb{E}_{\mathcal{T} \sim \mathfrak{T}(\theta)} \left[\sum_{T_i^+ \in \mathcal{T}} T_i^+(t) \right] \approx \frac{1}{J} \sum_{j=1}^J \sum_{T_i^+ \in \mathcal{T}^{(j)}} T_i^+(t) \quad (6)$$

where $\{T_i^+(t)\} =: \mathcal{T}^{(j)} \sim \mathfrak{T}(\theta) \forall j$ are sets of state variables of positively tested that were independently and randomly generated from the simulator $\mathfrak{T}(\theta)$ of our model. As indicated above, the expectation is approximated using J independent random roll-outs using Monte Carlo integration. Hence, the observations of functions $g_t(\theta)$ are stochastic and can be seen as noisy. We use the mean number of positive cases of J realizations to reduce the variance of function evaluations and be able to estimate its uncertainty. As a sum of independent random variables, the function $g_t(\theta)$ is normally distributed around the true expectation by the central limit theorem. We can use the empirical standard error of the mean as an estimate of observation noise in the surrogate model of g_t .

Our simulation \mathfrak{T} is stochastic not only due to different realizations of the counting processes, but in absence of real observations also due to randomly seeded infection states and random synthetic mobility traces $P_{i,k}(t)$. The various sources of stochasticity can be viewed as a form of regularization during parameter estimation, making the results more robust to different realizations of individual mobility patterns. Given the above, the T stochastic black-box functions can be viewed as one stochastic vector-valued black-box function $\mathbf{g}(\theta) \in \mathbb{R}^{|T|}$ with $\mathbf{g}(\theta)_t := g_t(\theta)$. All T black-box functions g_t share the same J random simulations in practice.

Objective function. Given a time horizon of T days, the objective we aim to *minimize* in our setting is the *sum of daily squared errors of cumulative positive cases* between simulations and real observations. This allows us to form a link between the spatiotemporal states of each individual of the simulation and aggregate longitudinal testing data. The squared error has been previously considered in parameter estimation [40]. Since BO algorithms usually consider the problem of global *maximization*, we negate our desired minimization loss and define the score $s(\mathbf{x}) = -\sum_{t=1}^T (c_t^{\text{true}} - \mathbf{x}_t)^2$ which we aim to maximize.

Let c_t^{true} be the cumulative number of real positive COVID-19 cases by day t as provided by the national authorities [42, 43]. Then, the objective f can be seen as a composition of the two functions s and \mathbf{g} . Note that, while the negative squared error score s is functionally known, the simulator \mathbf{g} computes the mean number of total positive cases across a time horizon as defined in Eq. 6 and viewed as a “black-box” function. Hence, the composite objective f to be maximized can be written as

$$f(\theta) = s(\mathbf{g}(\theta)) = -\sum_{t=1}^T (c_t^{\text{true}} - g_t(\theta))^2 \quad (7)$$

The fact that our objective f is a composite function of the score s and the high-dimensional \mathbf{g} allows the surrogate model to learn the black-box function \mathbf{g} directly rather than the scalar objective f . By recognizing and exploiting the compositionality of our black-box objective, we follow recent BO literature that has shown immense practical advantages in explicitly modeling compositionality [40, 41].

Knowledge gradient acquisition function. Measurements of the objective f are inherently noisy using our stochastic simulation. Thus, we employ the knowledge gradient (KG) [44, 45] acquisition function to navigate the proposals of new parameter settings. KG quantifies the expected increase in the maximum of the posterior mean of the modeled black-box function after an observation at a certain parameter setting of θ . The KG of measuring at θ is formally defined as

$$\text{KG}(\theta) := \mathbb{E}_{\mathbf{y} \sim p(\mathbf{g}(\theta) \mid \mathcal{D})} \left[\mu^*(\mathcal{D} \cup \{(\theta, \mathbf{y})\}) - \mu^*(\mathcal{D}) \right] \quad (8)$$

$$\mu^*(.) = \max_{\theta' \in \text{dom}(\theta)} \mathbb{E} [s(\mathbf{g}(\theta')) \mid .] \quad (9)$$

where $\mu^*(\mathcal{D} \cup \{(\theta, \mathbf{y})\})$ and $\mu^*(\mathcal{D})$ denote the maxima of the conditional means of the objective f given the observations \mathcal{D} under the surrogate model p , with the additional random observation (θ, \mathbf{y}) in the first term. Compared to simpler acquisition functions such as Expected Improvement, KG often shows improved performance and is well-suited for settings with noisy observations [41, 46].

Overall estimation procedure. Our parameter estimation procedure follows the typical Bayesian optimization paradigm of iterated cheap proposals and expensive function evaluations, repeatedly proposing new parameters based on the GP surrogate model of the objective. The overall procedure is summarized in Algorithm 3 of Appendix H. For proper initialization of the GP surrogate model and acquisition function, we evaluate the model at the first M samples of the $|\theta|$ dimensional quasi-random Sobol sequence [47], obtaining low-discrepancy points of initialization and giving the acquisition function an informative starting point. We use the BoTorch library [41] to implement our procedure and to optimize the knowledge gradient.

4 Experimental Design

We showcase our modeling framework using data from both rural and urban areas in Germany and Switzerland spanning a wide range of infection levels until today. More specifically, we experiment with two cities and

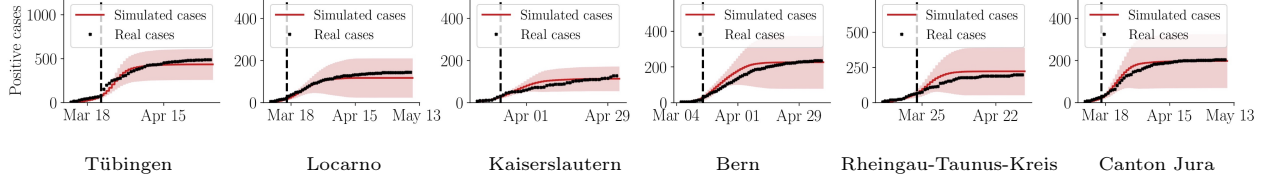


Figure 2: **Cumulative number of cases for the models of the considered regions.** The line represents the mean cumulative number of positively tested individuals over 48 random realizations of the simulations, the shaded regions correspond to two times the standard deviation. The dashed line represents the start of the “lockdown” measures, and the black line the real observed cases. Averaged over days of simulation, the mean absolute error (MAE) of predicted cases ranges between 10-30 cases across the six regions.

one district (Landkreis) in Germany – Tübingen, Kaiserslautern and the Landkreis of Rheingau-Taunus – and two cities and one state (Canton) in Switzerland – Bern, Locarno, and the Canton of Jura; see Table 3.

In our experiments, we use the efficient sampling algorithm for our model derived in Appendix E to simulate the spread of COVID-19 under a variety of interventions on two different epidemiological scenarios:

- **Scenario A (Initially uncontrolled):** *Early stage of the outbreak. After a reaction delay, governments aim to globally contain and suppress infections in the population. At the time of the interventions, there is already a significant number of infected individuals. Contact tracing is usually not in place yet.*

Setup: We simulate the spread of COVID-19 from the day when a given region had five to ten confirmed cases, typically in early March, until the end of the “lockdown” period, the period of time when most restrictive measures were in place.² We use heuristically computed initially infected seeds and assume that measures are in place *only* during the “lockdown” period, which starts approximately after two weeks of uncontrolled spread. Refer to Appendix F for state initialization in this scenario.

- **Scenario B (Continual suppression):** *Later stage of the epidemic. Measures taken by the governments have ended the first wave of infections. Local outbreaks occur due to imported cases, e.g., from visits to other regions. Contact tracing and localized interventions are employed as fine-grained tools for suppressing a resurgence of infections, i.e., a second wave.*

Setup: We simulate the spread of COVID-19 for 120 days without reference to a specific date range and assuming *five untraceable background exposures per week per 100,000 inhabitants* of a region in expectation.

In the absence of individual mobility data, which may become available once contact tracing systems are widely deployed, we generate realistic mobility traces $P_{i,k}(t)$ for all individuals $i \in \mathcal{V}$ and sites $k \in \mathcal{S}$ in each region using a variety of publicly available data sources, i.e., spatial distribution of site locations, as exemplified by Figure 1, high-resolution population density data, country-specific information about household structure [51, 52], and region-specific age demographics. Refer to Appendix G for additional details.

For each region, we estimate the transmission rates β_k and ξ due to infectious individuals at the sites they visit, in their households, as well as the mobility reduction p due to social distancing using Bayesian optimization. As explained in Section 3, our parameter estimation procedure uses publicly available COVID-19 data of daily cases in country-level administrative regions from the entire period of time described in *Scenario A* as its prediction target.³ To this end, we downscale the model and also simulate the corresponding business restrictions and closures that were in place during the “lockdown” period. Refer to Appendix H for additional information. To estimate the mortality and hospitalization rates per age group, we resort to previous studies [21] and COVID-19 case data [42, 43].

² This “lockdown” period started on March 23 and 16, 2020 and ended on May 3 and 10, 2020 in Germany and Switzerland, respectively [48–50].

³For cities, cases are scaled proportionally to its population for lack of more available information.

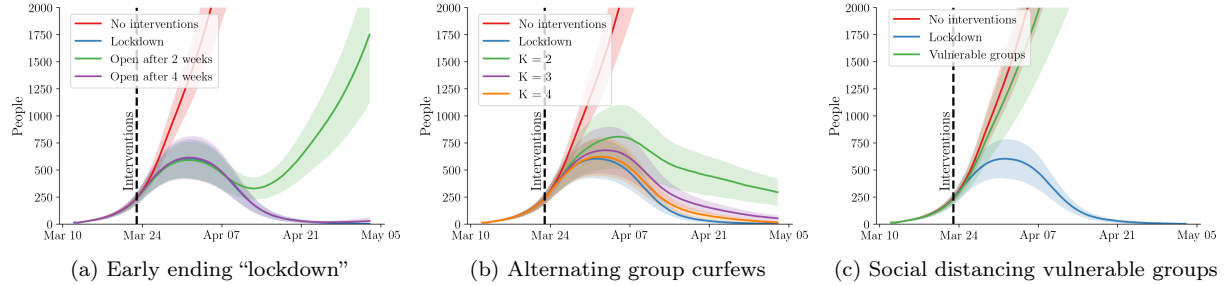


Figure 3: **Number of infected people for the model of Tübingen under different counterfactual what-if scenarios.** In panel (a), we implement the same restrictive measures that were in place during the “lockdown” period but reduce its length. In panel (b), the population is divided into K subgroups and, on each day, only one group out of K is allowed to follow their usual daily activities. In panel (c), the population over 60 years old follows the same social distancing measures that were in place during the “lockdown” period. In all panels, the lines represent the mean of 48 random realizations of the simulations and the shaded regions correspond to two times the standard deviation.

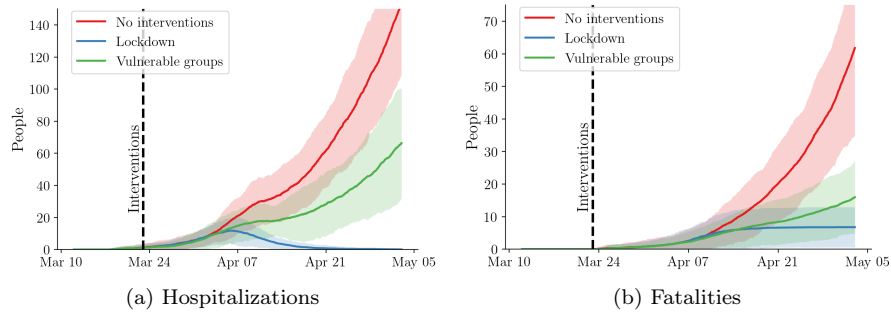


Figure 4: **Hospitalizations and fatalities for the model of Tübingen under social distancing of vulnerable groups.** In both panels, the lines represent the mean of 48 random realizations of the simulations and the shaded regions correspond to two times the standard deviation.

Finally, to abstract away from variable testing criteria implemented in different regions, we assume that only true symptomatic individuals are registered for testing unless stated otherwise and that the testing queue follows the first-in-first-out principle. Tests are assumed to have perfect accuracy, and positively tested individuals stop visiting sites and isolate themselves from their household members. Moreover, we set the reporting delay Δ_{test} to 48 hours, accounting for both the delay in self-reporting and the testing procedure itself. The testing rate $\lambda_{\text{test}}(t)$ per day is set to the inverse of the maximum daily increase in positive cases in the real observed COVID-19 data of the corresponding region.

5 Results

Using the estimated parameters β_k , ξ and p , we first validate that our model is able to faithfully characterize the observed real COVID-19 case data during the entire period of time described in *Scenario A*; see Figure 2. Refer to Table 6 in the appendix for the estimated parameter values. The results show that our models can consistently reproduce the overall longitudinal trend in real case data for all considered regions, and that the parameters estimated using the downscaled models are a good fit for the full-scale models. Appendix I discusses when parameter estimation using downscaled models might fail. Moreover, the results shown in Figure 8 suggest that the social distancing measures and business restrictions imposed on the population

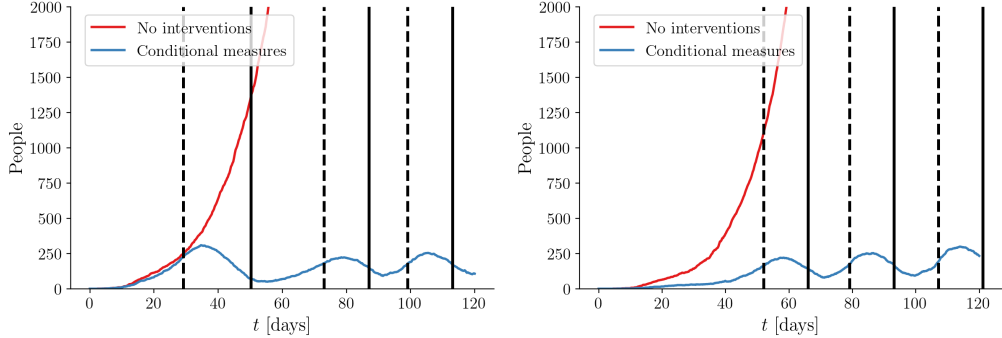


Figure 5: **Number of infected people in two single simulations of the model of Tübingen under conditional “lockdowns” based on weekly incidence.** Whenever the number of positive cases within 7 days exceeds the threshold of 50 per 100,000 inhabitants, we implement the same restrictive measures that were in place during the “lockdown” period in *Scenario A*. Dashed and solid vertical lines indicate beginning and ending of the conditional “lockdowns”, respectively.

during the lockdown period were effective in temporarily reducing R_t below the threshold of *one* both in Germany and Switzerland, a necessary condition for the epidemic to come to a halt.

First, we investigate to what extent containment of the first wave of infections in *Scenario A* would have been feasible using measures with lower impact on civil liberties and the economy. To this end, we explore three counterfactual “what-if” scenarios that implement milder containment measures than those that were in place during the “lockdown” period.

Early ending “lockdown”. We implement the same restrictive measures that were in place during the “lockdown” period both in Germany and Switzerland but reduce the their duration. Figure 3a summarizes the results for Tübingen and Figure 9 for all the considered towns and regions. The results suggest that, to end the first wave of infections, it should have been sufficient to maintain the “lockdown” period for just one month rather than two. However, they also show that a “lockdown” period of two weeks would be insufficient, except for the notable exception of the Landkreis of Rheingau-Taunus.

Alternating curfews for random subgroups. We divide the population into K subgroups and, on each day, we alternately prescribe curfews to $K - 1$ of the groups and only allow one group to follow their usual daily activities. Figure 3b summarizes the results for Tübingen and Figure 10 for all the considered towns and regions. The results suggest that, as long as the number of groups $K > 2$, this containment strategy would be effective at reducing both intra- and inter-group exposure events, as argued by previous work [53, 54], and the number of infected individuals would have followed a similar course as in the “lockdown” scenario. However, for $K = 2$ groups, the results are mixed. In all the considered German towns and regions, the strategy would still be relatively successful, however, in the Swiss city of Bern and the Canton of Jura, the number of infected individuals would have constantly increased.

Social distancing of vulnerable groups. The population over 60 years old, who typically suffers more complications from COVID-19 [42], follows the same social distancing measures that were in place during the “lockdown” period and the rest of the population follows their usual daily activities. Figures 3c and 4 summarize the results for Tübingen and Figure 11 for all the considered towns and regions. As one may have expected, the results suggest that this containment strategy would not end the first wave of infections. However, they also show that it would only modestly reduce the number of hospitalizations and fatalities, questioning the effectiveness of controversial policies that initially advocated for isolating only the people who are most endangered.

Next, we focus on *Scenario B* and investigate the effectiveness of adaptive containment measures that utilize testing and contact tracing to suppress a second wave of infections.

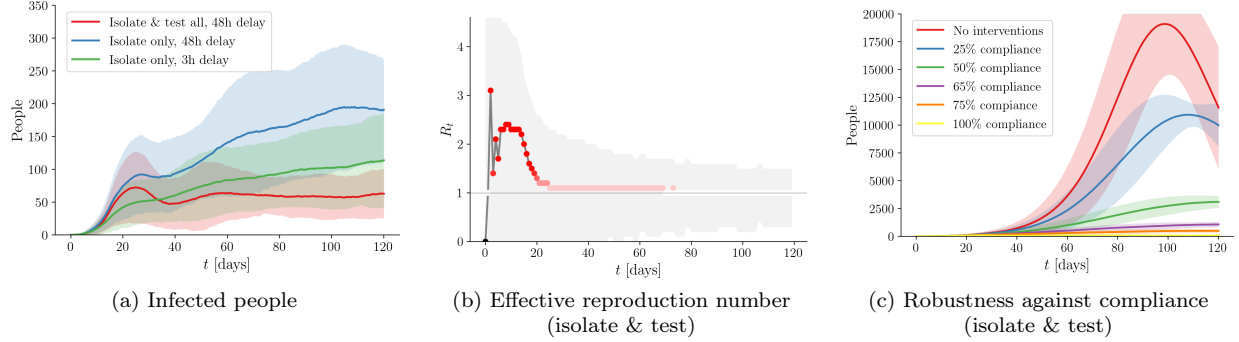


Figure 6: **Contact tracing for isolation and testing for the model of Tübingen.** Panel (a) shows the number of infected people whenever contact tracing is used for contact isolation and testing with different reporting delays Δ_{test} . Panel (b) shows the effective reproduction number R_t when contact tracing is used for isolation and testing. Panel (c) shows the number of infected people for the same setting under different levels of compliance. In panels (a) and (c), lines and shading indicate the mean and two times the standard deviations over 48 random roll-outs. In panels (b) and (c), the reporting delay is set to $\Delta_{\text{test}} = 48$ hours. In panel (b), the line represents the most likely estimate and shading represents high density areas.

Conditional “lockdowns” based on weekly incidence. Whenever the number of new cases within 7 days exceeds the threshold of 50 per 100,000 inhabitants, we implement the same restrictive measures that were in place during the “lockdown” period in *Scenario A*. This has been the strategy in place in Germany since May 6, 2020 [55]. Figure 5 shows the number of infected people over time during a single realization for Tübingen. As shown in Figure 12, we found qualitatively similar results across realizations for all the considered towns and regions. We observe that the repeated lifting of measures leads to fluctuations in the number of infected individuals, but the short “lockdowns” are able to quickly reduce the number of new cases below the desired threshold. While the typical length of the interventions is two weeks in Tübingen – with intermittent unrestricted phases of similar duration – we find that, e.g., in Bern, case-conditional “lockdowns” typically last for four weeks, with only three weeks without measures in between.

Contact tracing for isolation and testing. Whenever an individual is positively tested, we first use contact tracing to identify all their contacts in the ten days leading up to the positive test result and isolate them from everyone for 14 days, unless mentioned otherwise. We investigate to what extent the use of rapid testing [56], i.e., we set Δ_{test} to three hours, or further testing of contacts⁴ can increase the effectiveness of the above basic strategy. Finally, we evaluate the effectiveness of the contact tracing for isolation and testing under constraints on the compliance level and an advanced testing strategy. Figures 6 and 7 summarize our results for Tübingen and Figures 13 and 14 for all considered towns and regions. In Figures 6a and 13, we observe that the basic strategy, which only implements isolation of contacts, is already able to avoid a significant resurgence in infections in all towns and regions. Moreover, the use of rapid tests and further testing of contacts provide an additional reduction on the mean and variance of infection counts across random roll-outs. Interestingly, under further testing of contacts, the number of infected people over time reaches a steady state—the effective reproduction number R_t is pushed towards one, as shown in Figure 6b. In Figure 6c, we observe that the effectiveness of contact tracing gradually degrades with lower compliance due to the so-called “ x^2 problem” of adoption [22, 38], i.e., two parties needing to adopt contact tracing technology for the infection chain to be tracked. In Appendix J, we analyze an alternative strategy to identify contacts, called narrowcasting [57], which circumvents this problem. Finally, in Figures 7 and 14, we observe that, when testing only the top 20 contacts ranked according to *empirical probability of exposure* of Appendix D, it is possible to achieve the same reduction in infections as achieved when testing all contacts, even though the overall number of tests is reduced by 70-90% (47,927 to 8,821 tests in Tübingen).

⁴Here, we assume that the testing capacity is high enough for every traced contact to be tested.

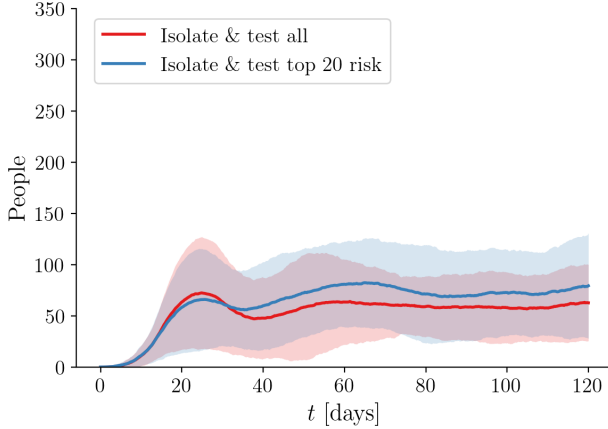


Figure 7: **Contact tracing for isolation with testing based on exposure risk.** Whenever we test only the top 20 contacts by their empirical probability of exposure as estimated from contact tracing, the overall number of tests is reduced by 70-90%. Lines and shading indicate the mean and two times the standard deviations over 48 random initializations.

6 Discussion

Motivated by the rapid development of contact tracing technology and the current COVID-19 outbreak, we have introduced a spatiotemporal epidemic model that uses temporal point processes to represent individual mobility patterns and the course of the disease for each individual in a population. Through an extensive case study using real COVID-19 data and mobility patterns from several cities and regions in Germany and Switzerland, we have shown that our model can be used to quantify the effects of contact tracing, testing, and a variety of containment measures in two different epidemiological scenarios. Our results reveal both qualitative and quantitative differences and similarities across geographically diverse areas spanning a wide range of levels of transmission until today, and demonstrate that our model may allow individuals and policy-makers to make more effective decisions. To facilitate this, we release an easy-to-use implementation of the entire framework necessary to perform experiments for any desired region of the world.

Several countries are deploying contact tracing technology, however, contact tracing data is not accessible to researchers as of today. Therefore, we have used geolocation data, high-resolution population density data, country-specific information about household structure and region-specific age demographics to generate realistic individual mobility traces. Once data from contact tracing technologies become accessible to researchers, we believe that our predictions will have lower variance and it will be possible to use our framework to identify areas with higher risk of infection in real time.

Beyond legal compliance and gaining societal acceptance, the use of epidemic models with high spatiotemporal resolution such as ours, as well as contact tracing technology, should respect each individual's privacy. In this context, it is important to highlight that, both during parameter estimation and contact tracing, we only need to compute the *duration* of contact that each individual had with an infected person—the identity of the infected person is not required. As a result, there are reasons to believe that such computations can be made in a decentralized and privacy-preserving manner [58, 59].

Finally, although our model has significantly greater spatiotemporal resolution than many of those in use today, we recommend to exercise caution when interpreting or using its results. Its predictions can only be faithfully considered when being aware of the high variance observed across random realizations. We advise against the implementation of testing and tracing strategies, social distancing measures, or business closures based solely on the predictions made by our model.

Acknowledgements

We thank the Robert-Koch-Institute, OpenStreetMaps and Facebook for providing data to make this work possible. We thank Brian Karrer from Facebook for his insightful comments and suggestions regarding Bayesian optimization, and Yannik Schaelte for useful comments on a preliminary version of this work. We thank Cansu Culha and the Stanford Future Bay Initiative as well as Pavol Harar from the University of Vienna for working with us to improve our open-source implementation. This work was supported in part by SNSF under grant number 200021-182407.

References

- [1] “The COVID tracking project.” <https://covidtracking.com/api/>, 2020. [Online; accessed March 27, 2020].
- [2] World Health Organization, “Coronavirus disease (COVID-2019) situation reports.” <https://www.who.int/emergencies/diseases/novel-coronavirus-2019/situation-reports/>, 2020. [Online; accessed March 27, 2020].
- [3] “COVID Safe Paths.” <http://safepaths.mit.edu>, 2020. [Online; accessed July 30, 2020].
- [4] “Zerobase – Privacy-First Contact Tracing for Communities.” <http://zerobase.io>, 2020. [Online; accessed July 30, 2020].
- [5] “DP3T - Decentralized Privacy-Preserving Proximity Tracing.” <https://github.com/DP-3T/documents>, 2020. [Online; accessed July 30, 2020].
- [6] Ministry of Health and Government Technology Agency, Singapore, “TraceTogether.” www.tracetogther.gov.sg, 2020. [Online; accessed July 30, 2020].
- [7] “Corona-Warn-App.” <https://www.coronawarn.app/en/>, 2020. [Online; accessed July 30, 2020].
- [8] D. Bernoulli, “Essai d’une nouvelle analyse de la mortalité causée par la petite vérole, et des avantages de l’inoculation pour la prévenir,” *Histoire de l’Acad., Roy. Sci.*, 1760.
- [9] K. Dietz and J. Heesterbeek, “Daniel Bernoulli’s epidemiological model revisited,” *Mathematical biosciences*, 2002.
- [10] W. Kermack and A. Mckendrick, “A contribution to the mathematical theory of epidemics,” *Proc. R. Soc.*, 2003.
- [11] R. Ross *et al.*, “An application of the theory of probabilities to the study of a priori pathometry. part i,” *Proc. R. Soc.*, 1916.
- [12] R. Ross, H. P. Hudson, *et al.*, “An application of the theory of probabilities to the study of a priori pathometry. part iii,” *Proc. R. Soc.*, 1917.
- [13] H. J. Ahn and B. Hassibi, “Global dynamics of epidemic spread over complex networks,” in *CDC*, 2013.
- [14] E. Cator and P. Van Mieghem, “Second-order mean-field susceptible-infected-susceptible epidemic threshold,” *Physical review E*, 2012.
- [15] D. Chakrabarti, Y. Wang, C. Wang, J. Leskovec, and C. Faloutsos, “Epidemic thresholds in real networks,” *ACM TISSEC*, 2008.
- [16] P. Van Mieghem, “The N-intertwined SIS epidemic network model,” *Computing*, 2011.
- [17] P. Van Mieghem, J. Omic, and R. Kooij, “Virus spread in networks,” *IEEE/ACM TON*, 2009.

[18] S. Benzell, A. Collis, and C. Nicolaides, “Rationing social contact during the covid-19 pandemic: Transmission risk and social benefits of us locations,” *Social Science Research Network (SSRN)*, 2020.

[19] J. Dehning, J. Zierenberg, F. P. Spitzner, M. Wibral, J. P. Neto, M. Wilczek, and V. Priesemann, “Inferring covid-19 spreading rates and potential change points for case number forecasts,” *arXiv preprint arXiv:2004.01105*, 2020.

[20] L. Di Domenico, G. Pullano, P. Coletti, N. Hens, and V. Colizza, “Expected impact of school closure and telework to mitigate covid-19 epidemic in france,” 2020.

[21] N. M. Ferguson, D. Laydon, G. Nedjati-Gilani, N. Imai, K. Ainslie, M. Baguelin, S. Bhatia, A. Boonyasiri, Z. Cucunubá, G. Cuomo-Dannenburg, *et al.*, “Impact of non-pharmaceutical interventions (npis) to reduce COVID-19 mortality and healthcare demand,” *London: Imperial College COVID-19 Response Team, March*, vol. 16, 2020.

[22] L. Ferretti, C. Wymant, M. Kendall, L. Zhao, A. Nurtay, D. G. Bonsall, and C. Fraser, “Quantifying dynamics of sars-cov-2 transmission suggests that epidemic control and avoidance is feasible through instantaneous digital contact tracing,” *Science*, 2020.

[23] R. Herbrich, R. Rastogi, and R. Vollgraf, “Crisp: A probabilistic model for individual-level covid-19 infection risk estimation based on contact data,” 2020.

[24] A. J. Kucharski, P. Klepac, A. J. K. Conlan, S. M. Kissler, M. L. Tang, H. Fry, J. R. Gog, W. J. Edmunds, J. C. Emery, G. Medley, J. D. Munday, T. W. Russell, Q. J. Leclerc, C. Diamond, S. R. Procter, A. Gimma, F. Y. Sun, H. P. Gibbs, A. Rosello, K. van Zandvoort, S. HuÃ©, S. R. Meakin, A. K. Deol, G. Knight, T. Jombart, A. M. Foss, N. I. Bosse, K. E. Atkins, B. J. Quilty, R. Lowe, K. Prem, S. Flasche, C. A. B. Pearson, R. M. G. J. Houben, E. S. Nightingale, A. Endo, D. C. Tully, Y. Liu, J. Villabona-Arenas, K. O'Reilly, S. Funk, R. M. Eggo, M. Jit, E. M. Rees, J. Hellewell, S. Clifford, C. I. Jarvis, S. Abbott, M. Auzenberg, N. G. Davies, and D. Simons, “Effectiveness of isolation, testing, contact tracing, and physical distancing on reducing transmission of SARS-CoV-2 in different settings: a mathematical modelling study,” *The Lancet Infectious Diseases*, 2020. Publisher: Elsevier.

[25] R. Li, S. Pei, B. Chen, Y. Song, T. Zhang, W. Yang, and J. Shaman, “Substantial undocumented infection facilitates the rapid dissemination of novel Coronavirus (SARS-CoV2),” *Science*, 2020.

[26] Q. Lin, S. Zhao, D. Gao, Y. Lou, S. Yang, S. S. Musa, M. H. Wang, Y. Cai, W. Wang, L. Yang, *et al.*, “A conceptual model for the coronavirus disease 2019 (covid-19) outbreak in wuhan, china with individual reaction and governmental action,” *International journal of infectious diseases*, vol. 93, pp. 211–216, 2020.

[27] S. M. Moghadas, A. Shoukat, M. C. Fitzpatrick, C. R. Wells, P. Sah, A. Pandey, J. D. Sachs, Z. Wang, L. A. Meyers, B. H. Singer, *et al.*, “Projecting hospital utilization during the covid-19 outbreaks in the united states,” *Proceedings of the National Academy of Sciences*, 2020.

[28] B. Vermeulen, A. Pyka, and M. Müller, “An agent-based policy laboratory for COVID-19 containment strategies.” <https://inno.uni-hohenheim.de/corona-modell>, 2020. [Online; accessed April 14, 2020].

[29] C. R. Wells, P. Sah, S. M. Moghadas, A. Pandey, A. Shoukat, Y. Wang, Z. Wang, L. A. Meyers, B. H. Singer, and A. P. Galvani, “Impact of international travel and border control measures on the global spread of the novel 2019 coronavirus outbreak,” *Proceedings of the National Academy of Sciences*, vol. 117, no. 13, pp. 7504–7509, 2020.

[30] A. L. Bertozzi, E. Franco, G. Mohler, M. B. Short, and D. Sledge, “The challenges of modeling and forecasting the spread of covid-19,” *Proceedings of the National Academy of Sciences*, vol. 117, no. 29, pp. 16732–16738, 2020.

[31] A. Aleta, D. MartÃn-Corral, A. Pastore y Piontti, M. Ajelli, M. Litvinova, M. Chinazzi, N. E. Dean, M. E. Halloran, I. M. Longini Jr, S. Merler, A. Pentland, A. Vespignani, E. Moro, and Y. Moreno, “Modelling the impact of testing, contact tracing and household quarantine on second waves of COVID-19,” *Nature Human Behaviour*, Aug. 2020.

[32] A. De, U. Upadhyay, and M. Gomez-Rodriguez, “Temporal point processes,” tech. rep., Technical report, Saarland University, 2019.

[33] E. Brochu, V. M. Cora, and N. de Freitas, “A tutorial on bayesian optimization of expensive cost functions, with application to active user modeling and hierarchical reinforcement learning,” 2010.

[34] D. R. Jones, M. Schonlau, and W. J. Welch, “Efficient global optimization of expensive black-box functions,” *Journal of Global optimization*, vol. 13, no. 4, pp. 455–492, 1998.

[35] J. Snoek, H. Larochelle, and R. P. Adams, “Practical bayesian optimization of machine learning algorithms,” in *Advances in neural information processing systems*, pp. 2951–2959, 2012.

[36] L. Lorch, H. Kremer, W. Trouleau, S. Tsirtsis, A. Szanto, B. Schölkopf, and M. Gomez-Rodriguez, “Data and code from “Quantifying the Effects of Contact Tracing, Testing, and Containment Measures.”” <https://github.com/covid19-model>, 2020. [Online; accessed July 24, 2020].

[37] N. van Doremalen, T. Bushmaker, D. Morris, M. Holbrook, A. Gamble, B. Williamson, A. Tamin, J. Harcourt, N. Thornburg, S. Gerber, J. Lloyd-Smith, E. de Wit, and V. Munster, “Aerosol and surface stability of HCoV-19 (SARS-CoV-2) compared to SARS-CoV-1,” *medRxiv*, 2020.

[38] J. Langford, “Critical issues in digital contract tracing,” 2020.

[39] O. O. Aalen, Ø. Borgan, and H. K. Gjessing, *Survival and Event History Analysis*. Springer New York, 2008.

[40] R. Astudillo and P. I. Frazier, “Bayesian optimization of composite functions,” 2019.

[41] M. Balandat, B. Karrer, D. R. Jiang, S. Daulton, B. Letham, A. G. Wilson, and E. Bakshy, “Botorch: Programmable bayesian optimization in pytorch,” 2019.

[42] Robert Koch-Institut (RKI), dl-de/by-2-0, “RKI COVID19 data set.” <https://npgeo-corona-npgeo-de.hub.arcgis.com/datasets/>, 2020. [Online; accessed July 13, 2020].

[43] Bundesamt für Gesundheit, Schweiz, “BAG COVID19 situation summary.” <https://www.bag.admin.ch/bag/en/home/krankheiten/ausbrueche-epidemien-pandemien/aktuelle-ausbrueche-epidemien/novel-cov/situation-schweiz-und-international.html>, 2020. [Online; accessed July 13, 2020].

[44] P. I. Frazier, W. B. Powell, and S. Dayanik, “A knowledge-gradient policy for sequential information collection,” *SIAM J. Control Optim.*, vol. 47, p. 2410–2439, Sept. 2008.

[45] J. Wu and P. Frazier, “The parallel knowledge gradient method for batch bayesian optimization,” in *Advances in Neural Information Processing Systems 29* (D. D. Lee, M. Sugiyama, U. V. Luxburg, I. Guyon, and R. Garnett, eds.), pp. 3126–3134, Curran Associates, Inc., 2016.

[46] P. I. Frazier, “A tutorial on bayesian optimization,” 2018.

[47] I. Sobol, “On the distribution of points in a cube and the approximate evaluation of integrals,” *USSR Computational Mathematics and Mathematical Physics*, vol. 7, no. 4, pp. 86 – 112, 1967.

[48] Land Baden-Württemberg, “Verordnung der Landesregierung über infektionsschützende Massnahmen gegen die Ausbreitung des Virus SARS-CoV-2 (Corona-Verordnung).” <https://www.baden-wuerttemberg.de/de/service/aktuelle-infos-zu-corona/aktuelle-corona-verordnung-des-landes-baden-wuerttemberg/>, 2020. [Online; accessed April 14, 2020].

[49] Bundesländer der Bundesrepublik Deutschland, “Corona-Regelungen in den Bundesländern.” <https://www.bundesregierung.de/breg-de/themen/coronavirus/corona-bundeslaender-1745198>, 2020. [Online; accessed July 09, 2020].

[50] Der Schweizerische Bundesrat, “Verordnung 2 über Massnahmen zur Bekämpfung des Coronavirus (COVID-19) (COVID-19-Verordnung 2).” <https://www.admin.ch/opc/de/classified-compilation/20200744/index.html>, 2020. [Online; accessed July 09, 2020].

[51] Statistisches Bundesamt, Deutschland, “Households, by type of household. Long-term series with annual data from 1961..” <https://www.destatis.de/EN/Themes/Society-Environment/Population/Households-Families/Tables/lrb bev05.html>, 2020. [Online; accessed May 16, 2020].

[52] Bundesamt für Statistik, Schweiz, “Households.” <https://www.bfs.admin.ch/bfs/de/home/statistiken/bevoelkerung/stand-entwicklung/haushalte.html>, 2020. [Online; accessed May 16, 2020].

[53] O. Karin, Y. M. Bar-On, T. Milo, I. Katzir, A. Mayo, Y. Korem, B. Dudovich, E. Yashiv, A. J. Zehavi, N. Davidovich, *et al.*, “Adaptive cyclic exit strategies from lockdown to suppress covid-19 and allow economic activity,” *medRxiv*, 2020.

[54] D. Meidan, R. Cohen, S. Haber, and B. Barzel, “An alternating lock-down strategy for sustainable mitigation of covid-19,” *arXiv preprint arXiv:2004.01453*, 2020.

[55] Bundesregierung Deutschland, “Telefonschaltkonferenz der Bundeskanzlerin mit den Regierungschefinnen und Regierungschefs der Länder am 6. Mai 2020.” <https://www.bundesregierung.de/resource/blob/973812/1750986/fc61b6eb1fc1d398d66cfea79b565129/2020-05-06-mpk-beschluss-data.pdf>, 2020. [Online; accessed July 18, 2020].

[56] European Center for Disease Prevention and Control, “An overview of the rapid test situation for COVID-19 diagnosis in the eu/eea.” <https://www.ecdc.europa.eu/sites/default/files/documents/Overview-rapid-test-situation-for-COVID-19-diagnosis-EU-EEA.pdf>, 2020. [Online; accessed July 18, 2020].

[57] J. Chan, S. Gollakota, E. Horvitz, J. Jaeger, S. Kakade, T. Kohno, J. Langford, J. Larson, S. Singanamalla, J. Sunshine, *et al.*, “Pact: Privacy sensitive protocols and mechanisms for mobile contact tracing,” *arXiv preprint arXiv:2004.03544*, 2020.

[58] M. Nanni, G. Andrienko, C. Boldrini, F. Bonchi, C. Cattuto, F. Chiaromonte, G. Comandé, M. Conti, M. Coté, F. Dignum, V. Dignum, J. Domingo-Ferrer, F. Giannotti, R. Guidotti, D. Helbing, J. Kertesz, S. Lehmann, B. Lepri, P. Lukowicz, A. Monreale, K. Morik, N. Oliver, A. Passarella, A. Passerini, D. Pedreschi, A. Pentland, F. Pratesi, S. Rinzivillo, S. Ruggieri, A. Siebes, R. Trasarti, J. van den Hoven, and A. Vespignani, “Give more data, awareness and control to individual citizens, and they will help COVID-19 containment,” 2020.

[59] C. Troncoso *et al.*, “Decentralized privacy-preserving proximity tracing.” <https://github.com/DP-3T/documents/blob/master/DP3T%20White%20Paper.pdf>, 2020. [Online; accessed April 14, 2020].

[60] S. A. Lauer, K. H. Grantz, Q. Bi, F. K. Jones, Q. Zheng, H. R. Meredith, A. S. Azman, N. G. Reich, and J. Lessler, “The Incubation Period of Coronavirus Disease 2019 (COVID-19) From Publicly Reported Confirmed Cases: Estimation and Application,” *Annals of Internal Medicine*, 2020.

[61] N. M. Linton, T. Kobayashi, Y. Yang, K. Hayashi, A. R. Akhmetzhanov, S.-m. Jung, B. Yuan, R. Kinoshita, and H. Nishiura, “Incubation period and other epidemiological characteristics of 2019 novel Coronavirus infections with right truncation: A statistical analysis of publicly available case data,” *Journal of Clinical Medicine*, vol. 9, no. 2, 2020.

[62] Robert Koch-Institut (RKI), “Epidemiologisches Bulletin des Robert Koch-Instituts (Ausgabe 15/2020).” https://www.rki.de/DE/Content/Infekt/EpidBull/Archiv/2020/Ausgaben/15_20.pdf?__blob=publicationFile, 2020. [Online; accessed April 13, 2020].

[63] H. Nishiura, T. Kobayashi, T. Miyama, A. Suzuki, S. Jung, K. Hayashi, R. Kinoshita, Y. Yang, B. Yuan, A. R. Akhmetzhanov, and N. M. Linton, “Estimation of the asymptomatic ratio of novel coronavirus infections (covid-19),” *medRxiv*, 2020.

[64] E. Lavezzo, E. Franchin, C. Ciavarella, G. Cuomo-Dannenburg, L. Barzon, C. Del Vecchio, L. Rossi, R. Manganelli, A. Loregian, N. Navarin, D. Abate, M. Sciro, S. Merigliano, E. Decanale, M. C. Vanuzzo, F. Saluzzo, F. Onelia, M. Pacenti, S. Parisi, G. Carretta, D. Donato, L. Flor, S. Cocchio, G. Masi, A. Sperduti, L. Cattarino, R. Salvador, K. A. Gaythorpe, A. R. Brazzale, S. Toppo, M. Trevisan, V. Baldo, C. A. Donnelly, N. M. Ferguson, I. Dorigatti, and A. Crisanti, “Suppression of covid-19 outbreak in the municipality of vo, italy,” *medRxiv*, 2020.

[65] L. Tindale, M. Coombe, J. E. Stockdale, E. Garlock, W. Y. V. Lau, M. Saraswat, Y.-H. B. Lee, L. Zhang, D. Chen, J. Wallinga, and C. Colijn, “Transmission interval estimates suggest pre-symptomatic spread of covid-19,” *medRxiv*, 2020.

[66] World Health Organization, “Report of the who-china joint mission on Coronavirus disease 2019 (covid-19).” <https://www.who.int/docs/default-source/coronavirus/who-china-joint-mission-on-covid-19-final-report.pdf>, 2020. [Online; accessed April 12, 2020].

[67] “Facebook Data for Good.” <https://dataforgood.fb.com>, 2020. [Online; accessed July 27, 2020].

[68] “OpenStreetMap.” <https://www.openstreetmap.org/>, 2020. [Online; accessed August 5, 2020].

[69] L. M. A. Bettencourt and R. M. Ribeiro, “Real time bayesian estimation of the epidemic potential of emerging infectious diseases,” *PLOS ONE*, vol. 3, pp. 1–9, 05 2008.

[70] K. Systrom, “Estimating covid-19’s r_t in real-time.” <https://github.com/k-sys/covid-19>, 2020.

[71] X. He, E. H. Y. Lau, P. Wu, X. Deng, J. Wang, X. Hao, Y. C. Lau, J. Y. Wong, Y. Guan, X. Tan, X. Mo, Y. Chen, B. Liao, W. Chen, F. Hu, Q. Zhang, M. Zhong, Y. Wu, L. Zhao, F. Zhang, B. J. Cowling, F. Li, and G. M. Leung, “Temporal dynamics in viral shedding and transmissibility of COVID-19,” *Nature Medicine*, vol. 26, pp. 672–675, May 2020.

[72] R. Woelfel, V. M. Corman, W. Guggemos, M. Seilmaier, S. Zange, M. A. Mueller, D. Niemeyer, P. Vollmar, C. Rothe, M. Hoelscher, T. Bleicker, S. Bruenink, J. Schneider, R. Ehmann, K. Zwirglmaier, C. Drosten, and C. Wendtner, “Clinical presentation and virological assessment of hospitalized cases of Coronavirus disease 2019 in a travel-associated transmission cluster,” *medRxiv*, 2020.

[73] D. Wang, B. Hu, C. Hu, F. Zhu, X. Liu, J. Zhang, B. Wang, H. Xiang, Z. Cheng, Y. Xiong, Y. Zhao, Y. Li, X. Wang, and Z. Peng, “Clinical Characteristics of 138 Hospitalized Patients With 2019 Novel Coronavirus-Infected Pneumonia in Wuhan, China,” *JAMA*, vol. 323, no. 11, pp. 1061–1069, 2020.

A Household infections

If information about the households $\mathcal{H}(i)$ that each individual $i \in \mathcal{V}$ belongs to is available, then one can account for infections within the households by adding the following base rate $\lambda_{\mathcal{H}(i)}(t)$ to the conditional intensity function $\lambda_i^*(t)$ of the exposure counting process $N_i(t)$:

$$\lambda_{\mathcal{H}(i)}(t) = \xi \sum_{j \in \mathcal{H}(t) \setminus i} \int_{t-\delta}^t (I_j^s(\tau) + I_j^p(\tau) + \mu I^a(\tau)) e^{-\gamma(t-\tau)} \prod_{k \in \mathcal{S}} (1 - P_{i,k}(\tau)) \prod_{k \in \mathcal{S}} (1 - P_{j,k}(\tau)) d\tau \quad (10)$$

where $\xi \geq 0$ is the transmission rate due to any presymptomatic and symptomatic individuals within households. This functional form of intensity function models our assumption that individuals within a household are in contact as long as they are not visiting any site.

Exposure events caused by the household exposure rate $\lambda_{\mathcal{H}(i)}(t)$ can be sampled analogously to the principles for sampling exposure times introduced in Appendix E, and their superposition with exposures at sites is handled correspondingly by the priority queue invariant.

B Disease-specific time-to-event distributions

We define the time-to-event distributions of the disease-specific counting processes $M_i(t)$, $R_i^a(t)$, $R_i^s(t)$, $W_i(t)$, $Y_i(t)$, and $Z_i(t)$, which do not depend on the mobility model, following the recent literature on COVID-19. More specifically, we consider the functional form of the intensity functions to be those of log-normal time-to-event distributions ($\log \mathcal{N}$) shifted to start at the time $E_i(t)$, $I_i^p(t)$, $I_i^a(t)$ or $I_i^s(t)$ become one, respectively. Table 2 gives more details about each of these distributions, including the specific work which we refer to for the distribution parameters. Whenever literature results on COVID-19 were only reported using mean or median estimates of times, we use log-normal distributions with corresponding normal parameters to define an approximate distribution, often consulting various sources. The log-normal distribution is commonly used to model event times in this context [60, 61].

C Contact tracing

When an individual i is tested positive, a subset of individuals previously in contact with i could be isolated or advised to seek testing. Under our model, the set of individuals $\mathcal{C}_{[t_0, t_f]}(i)$ who had contact with individual i during a time window $[t_0, t_f]$ at any possible site can be traced by both location-based and proximity-based tracing systems. A location-based contact tracing system records the times when an individual i checks in at different sites $k \in \mathcal{S}$, *i.e.*, it observes $P_{i,k}(t)$. Therefore, it can identify the set of individuals $\mathcal{C}_{[t_0, t_f]}(i)$ who had contact with individual i during a time window $[t_0, t_f]$ at any possible site, *i.e.*

$$\mathcal{C}_{[t_0, t_f]}(i) = \left\{ j \in \mathcal{V} \mid \sum_{k \in \mathcal{S}} \int_{t_0}^{t_f} P_{i,k}(t') \int_{t'-\delta}^{t'} P_{j,k}(\tau) e^{-\gamma(t'-\tau)} d\tau dt' > 0 \right\} \quad (11)$$

where the integral accounts for environmental transmission contacts at each site [37], analogous to the exposure rate λ^* .

By contrast, a proximity-based contact tracing system only records the times when a pair of individuals i and j have met, *i.e.*, have been physically close to each other, during a time window $[t_0, t_f]$. For simplicity, we overload notation and define $P_{i,j}(t) := \sum_{k \in \mathcal{S}} P_{i,k}(t) P_{j,k}(t) \in \{0, 1\}$ as the indicator of contact between individuals i and j . Observing $P_{i,j}(t)$, the authority can again identify the set of individuals $\mathcal{C}_{[t_0, t_f]}(i)$ who had contact with individual i during a time window $[t_0, t_f]$, *i.e.*

$$\mathcal{C}_{[t_0, t_f]}(i) = \left\{ j \in \mathcal{V} \mid \int_{t_0}^{t_f} P_{i,j}(t') dt' > 0 \right\} \quad (12)$$

where in contrast with Eq. 11 environmental transmission contacts cannot be tracked. Authorities could in principle resort to data from Bluetooth beacons to overcome this limitation of proximity-based contact tracing systems [38].

D Testing based on empirical probability of exposure

Once a contact tracing system has identified the contacts $\mathcal{C}_{[t_0, t_f]}(i)$ of individual i , different contact tracing policies can be implemented in various contexts. In this work, we consider the possibility of allocating tests based on the empirical exposure probability of contacts of an infectious person, which can be straightforwardly estimated using our framework. We define the *empirical risk testing policy* $\pi_{\text{test}}^{\text{risk}}$ as the allocation of tests only to the top K individuals j of the contacts $\mathcal{C}_{[t_0, t_f]}(i)$ ranked by their empirical probability of exposure $\hat{p}_{j \leftarrow i}([t_0, t_f])$ during a time window $[t_0, t_f]$ associated with i in the process $N_j(t)$:

$$\hat{p}_{j \leftarrow i}([t_0, t_f]) = \begin{cases} 1 - \exp \left(- \sum_{k \in \mathcal{S}} \int_{t_0}^{t_f} P_{j,k}(t') \int_{t'-\delta}^{t'} P_{i,k}(\tau) e^{-\gamma(t'-\tau)} d\tau dt' \right) & \text{location-based tracing} \\ 1 - \exp \left(- \int_{t_0}^{t_f} P_{i,j}(t') dt' \right) & \text{proximity-based tracing} \end{cases} \quad (13)$$

where the notation is overloaded for proximity-based tracing. While the isolation of contacts via tracing is generally not capacity-constrained, testing resources are often initially limited in practice [62]. Hence, we study the empirical effect of this advanced testing policy in our experiments. Disregarding second order effects and inaccuracies in estimating the empirical probability of exposure, the empirical risk testing policy can be interpreted as a greedy allocation of tests under limited resources. We leave the consideration of more sophisticated contact tracing policies for future work.

E Sampling algorithm

In this section, we describe how to generate realizations of the model by implementing the principles of superposition and thinning [32, 39] efficiently in a global context using one single priority queue of temporal events for all individuals in the model. The resulting sampling procedure is summarized as Algorithms 1 and 2.

E.1 Algorithmic backbone

First, note that the state variables $\mathbb{S}(t) = \{S_i(t), E_i(t), I_i^a(t), I_i^p(t), I_i^s(t), H_i(t), R_i(t), D_i(t)\}_{i \in \mathcal{V}}$ in the SDEs of the model change at – and only change at – *jumps* of the counting processes $\mathbb{C}(t) = \{N_i(t), M_i(t), R_i^a(t), R_i^s(t), W_i(t), Y_i(t), Z_i(t)\}_{i \in \mathcal{V}}$. Since these state transitions happen at specific points in continuous time, notice that all state variables $\mathbb{S}(t)$ are *constant between two consecutive jumps*, when considering all arrival times of all counting processes $\mathbb{C}(t)$ on *one* timeline in temporally sorted order. This leads us to the backbone principle for generating realizations of our model. We initialize the state variables $\mathbb{S}(0)$, compute the next time of state transition for each individual $i \in \mathcal{V}$, and push these transition events onto one single temporally-sorted priority queue Q . Then, the algorithm loops repeatedly through (i) popping the next event e from Q ; (ii) updating the corresponding state of individual i associated with e ; (iii) sampling the next time t of state transition e' for i ; and (iv) pushing e' to Q with priority t .

What remains to be shown is how to sample the state transition times for individual i given the state $\mathbb{S}(t)$ of everyone in the population. As explained in the model section of the paper, we fix the time-to-event distributions of all non-exposure related processes $\mathbb{C}(t) \setminus \{N_i(t)\}_{i \in \mathcal{V}}$ to independent, easy-to-sample distributions that were estimated by clinical COVID-19 literature. Hence, sampling the times of exposure $N_i(t)$ remains the central difficulty, as the intensities $\lambda_i^*(t)$ of the counting processes are interacting with all other state variables $\mathbb{S}(t)$ through the mobility model $P_{i,k}(t)$.

Algorithm 1 Sampling algorithm for model simulation

Input: Initial state variables at $t = 0$, location traces $P_{i,k}(t)$, parameters $\gamma, \delta, \alpha_a, \alpha_b, \alpha_h, \mu$ and β_k , hazard functions $\lambda_{-}(t)$

- 1: $t_{\text{now}} \leftarrow 0, S_i \leftarrow 1, Q \leftarrow$ priority queue processing in temporal order of events
- 2: **for** all $i \in \mathcal{V}$ s.t. $S_i = 0$ **do**
- 3: Push next state transition $(0, _, i, \emptyset)$ to Q (see below)
- 4: **while** Q not empty **do**
- 5: $(t_{\text{now}}, e, i, j, k) \leftarrow$ pop earliest from Q ▷ Event is (time of event, transition, i , infector, site)
- 6: **if** e is dE and $R_j(t_{\text{now}}) = 0$ and $D_j(t_{\text{now}}) = 0$ and $S_i = 1$ **then** ▷ Person i exposed by infector j
- 7: **if** $\text{INTERVENTIONS}(i, j, k, t_{\text{now}})$ **then**
- 8: Call Algorithm 2 with arguments $(P, j, i, t_{\text{now}}, r = 1 - (1 - \mu)I_j^a(t_{\text{now}}))$ ▷ Reject and re-sample
- 9: **else**
- 10: $E_i \leftarrow 1, S_i \leftarrow 0, \Delta_M \sim \text{Expo}(\lambda_M(t_{\text{now}})), u \sim \text{Unif}(0, 1)$
- 11: **if** $u \leq \alpha_a$ **then**
- 12: Push $(t_{\text{now}} + \Delta_M, dI^a, i, \emptyset)$ event to Q
- 13: **else**
- 14: Push $(t_{\text{now}} + \Delta_M, dI^p, i, \emptyset)$ event to Q
- 15: **else if** e is dI^p **then** ▷ Person i pre-symptomatic
- 16: $I_i^p \leftarrow 1, E_i \leftarrow 0, \Delta_Z \sim \text{Expo}(\lambda_W(t_{\text{now}}))$
- 17: Push $(t_{\text{now}} + \Delta_Z, dI^s, i, \emptyset)$ event to Q
- 18: **for** u such that $S_u = 1$ **do**
- 19: Call Algorithm 2 with arguments $(P, i, u, t_{\text{now}}, r = 1)$
- 20: **else if** e is dI^s **then** ▷ Person i symptomatic
- 21: $I_i^s \leftarrow 1, I_i^p \leftarrow 0, u, v \sim \text{Unif}(0, 1)$
- 22: **if** $u \leq \alpha_h$ **then**
- 23: $\Delta_Y \sim \text{Expo}(\lambda_Y(t_{\text{now}})), \text{Push } (t_{\text{now}} + \Delta_Y, dH, i, \emptyset)$
- 24: **if** $v \leq \alpha_b$ **then**
- 25: $\Delta_Z \sim \text{Expo}(\lambda_Z(t_{\text{now}})), \text{Push } (t_{\text{now}} + \Delta_Z, dD, i, \emptyset)$ event to Q
- 26: **else**
- 27: $\Delta_R \sim \text{Expo}(\lambda_{R^s}(t_{\text{now}})), \text{Push } (t_{\text{now}} + \Delta_R, dR, i, \emptyset)$ event to Q
- 28: **else if** e is dI^a **then** ▷ Person i asymptomatic
- 29: $I_i^a \leftarrow 1, E_i \leftarrow 0, \Delta_R \sim \text{Expo}(\lambda_{R^a}(t_{\text{now}}))$
- 30: Push $(t_{\text{now}} + \Delta_R, dR, i, \emptyset)$ event to Q
- 31: **for** u such that $S_u = 1$ **do**
- 32: Call Algorithm 2 with arguments $(P, i, u, t_{\text{now}}, r = \mu)$
- 33: **else if** e is dH **then** ▷ Person i hospitalized
- 34: $H_i \leftarrow 1$
- 35: **else if** e is dR **then** ▷ Person i resistant
- 36: $R_i \leftarrow 1, I_i^a \leftarrow 0, I_i^s \leftarrow 0, H_i \leftarrow 0$
- 37: **else if** e is dD **then** ▷ Person i deceased
- 38: $D_i \leftarrow 1, I_i^s \leftarrow 0, H_i \leftarrow 0$

E.2 Sampling exposure times

To sample the time of exposure of individual i , we need to sample the time-to-event of the next event of exposure counting process $N_i(t)$ with intensity $\lambda_i^*(t)$. To this end, we first decompose the intensity $\lambda_i^*(t)$ into a sum of contributions $\lambda_{j \rightarrow i}^*(t)$ caused by other individuals j :

$$\begin{aligned} \lambda_i^*(t) &= \sum_{k \in \mathcal{S}} \beta_k P_{i,k}(t) \sum_{j \in \mathcal{V} \setminus \{i\}} \int_{t-\delta}^t K_{j,k}(\tau) e^{-\gamma(t-\tau)} d\tau = \sum_{j \in \mathcal{V} \setminus \{i\}} \sum_{k \in \mathcal{S}} \beta_k P_{i,k}(t) \int_{t-\delta}^t K_{j,k}(\tau) e^{-\gamma(t-\tau)} d\tau \\ &=: \sum_{j \in \mathcal{V} \setminus \{i\}} \lambda_{j \rightarrow i}^*(t), \end{aligned} \quad (14)$$

where note the last summation over $j \in \mathcal{V} \setminus \{i\}$ is *sparse* as it effectively indexes over *contacts* of individuals i at times in the future, since $\lambda_{j \rightarrow i}^*(t) = 0$ when i and j are not in contact directly or j left site $k \in \mathcal{S}$ more than δ -time before i arrived.

By the decomposition of $N_i(t)$ above, the counting process $N_i(t)$ can be seen as a *superposition* of counting processes $N_{j \rightarrow i}(t)$ with rates $\lambda_{j \rightarrow i}^*(t)$, i.e. that $N_i(t) = \sum_{j \in \mathcal{V} \setminus \{i\}} N_{j \rightarrow i}(t)$. This implies that the *first* arrival

Algorithm 2 Pushes next event of individual i exposing individual j in time window $[t, T]$. This procedure considers the contribution $\lambda_{i \rightarrow j}^*(t)$ in Eq. 14 of individual i to rate $\lambda_j^*(t)$ alone. Implements thinning as described in Appendix E to obtain sound time-to-event sample τ of counting process with rate $\lambda_{i \rightarrow j}^*(t)$. Priority queue Q induces superposition to obtain a correct sample of $N_j(t)$ in Algorithm 1.

Input: P, i, j, t, r

- 1: **procedure** INCONTACT(u, v, τ)
- 2: **return** True **if** $\exists k \in \mathcal{S}$ s.t. (1) $P_{u,k}(\tau) = 1$ and (2) $\exists \tau' \in [\tau - \delta, \tau]$ s.t. $P_{v,k}(\tau') = 1$ **else return** False
- 3: **procedure** CONTACTSITE(u, v, τ)
- 4: **return** k **if** $\exists k \in \mathcal{S}$ s.t. (1) $P_{u,k}(\tau) = 1$ and (2) $\exists \tau' \in [\tau - \delta, \tau]$ s.t. $P_{v,k}(\tau') = 1$ **else return** \emptyset
- 5: **procedure** NEXTCONTACT(u, v, τ)
- 6: **return** $\min_{\tau' > \tau} \tau'$ s.t. INCONTACT(u, v, τ')
- 7: **procedure** WILLBEINCONTACT(u, v, τ)
- 8: **return** True **if** there exists $\tau' \in [\tau, T]$ s.t. INCONTACT(u, v, τ') **else return** False
- 9: $\tau \leftarrow t$
- 10: **while** WILLBEINCONTACT(j, i, τ) **do**
- 11: $b \leftarrow$ INCONTACT(j, i, τ)
- 12: **if not** b **then**
- 13: $\tau \leftarrow$ NEXTCONTACT(j, i, τ)
- 14: $\Delta_{E_j} \sim \text{Expo} \left(\max_k \{\beta_k\} r \int_{\tau - \delta}^{\tau} e^{-\gamma(\tau - v)} dv \right)$
- 15: $\tau \leftarrow \tau + \Delta_{E_j}$
- 16: **if** INCONTACT(j, i, τ) **then**
- 17: $k \leftarrow$ CONTACTSITE(j, i, τ)
- 18: $p \leftarrow \left(\beta_k \int_{\tau - \delta}^{\tau} e^{-\gamma(\tau - v)} P_{i,k}(v) dv \right) / \left(\max_k \{\beta_k\} \int_{\tau - \delta}^{\tau} e^{-\gamma(\tau - v)} dv \right)$
- 19: $u \sim \text{Unif}(0, 1)$
- 20: **if** $u \leq p$ **then**
- 21: Push (τ, dE, j, i) event to Q
- 22: **break**

of the counting process $N_i(t)$ is the *minimum* of the first arrivals of all processes $N_{j \rightarrow i}(t)$ [32, 39]. Then, as we already have the temporally-sorted priority queue Q in place, we can use its ordering invariant to process the valid exposure events of individuals on the fly. Whenever any individual j becomes infectious – either via $I_j^a = 1$ or $I_j^p = 1$ – we sample the next exposure event that j causes at rate $\lambda_{j \rightarrow i}^*(t)$ for every individual i which j will have contact with in the future, and push this event onto the priority queue Q . When an exposure event e for individual i is popped off the queue in step (i), we only have to check that e is the *first* exposure event of i in the simulation by verifying that $S_i(t) = 0$, discarding all subsequent exposure events for i that get popped from Q by finding $S_i(t) = 1$.

Moreover, to sample the first time to event for each counting process $N_{j \rightarrow i}(t)$, we use the principles of superposition and thinning [32, 39] as well as the memoryless property of the exponential distribution. The intensity $\lambda_{j \rightarrow i}^*(t)$ only has intervals of non-zero rate whenever j has infectious contact with i , either by meeting i at a site $k \in \mathcal{S}$ directly or by leaving less than δ -time before i arrives. Note that an upper bound on the individual exposure intensity is $\sup_{t \in [0, T]} \lambda_{j \rightarrow i}^*(t) = \max_{k \in \mathcal{S}} \{\beta_k (1 - \exp(-\gamma\delta)) / \gamma\} =: \lambda_{j \rightarrow i, \max}^*$ by Eq. 14. Thus, we can sample the next event time after time t by initializing $t' = t$ and repeating the following two steps until the first acceptance of t' : (i) add $\tau \sim \text{Expo}(\lambda_{j \rightarrow i, \max}^*)$ to t' ; (ii) accept with probability $\lambda_{j \rightarrow i}^*(t') / \lambda_{j \rightarrow i, \max}^*$. By the process called *thinning*, t' is a sound random sample of the time to the next event of $N_{j \rightarrow i}^*(t)$ [32].

The procedure is made more efficient by skipping over periods of $\lambda_{j \rightarrow i}^*(t) = 0$ whenever t in the above sampling loop reaches a zero-rate window in step (ii), which is sound by viewing the process $N_{j \rightarrow i}(t)$ itself as a superposition of sub-processes, one for each non-zero interval of intensity, and skipping the initial zero-rate period of sampling from such a sub-process by the memoryless property of the exponential distribution.⁵

⁵If $T \sim \text{Expo}(\lambda)$, then $P(T \geq t + s \mid T \geq s) = P(T \geq t)$.

E.3 Thinning

While the above handles all exposures caused by individuals that become infectious, it can happen that an infectious individual j has recovered from COVID-19 at the time an exposure event e caused by j for another person is popped off the queue Q . Note that if j recovers, i.e. $R_j(t) = 1$, then $\lambda_{j \rightarrow i}^*(t) = 0$ in Eq. 14 for the exposure event that was added to Q earlier in the simulation when $\lambda_{j \rightarrow i}^*(t) > 0$. Such an exposure event e simply has to be discarded by the principle of thinning, which can be easily checked on the fly by verifying that $R_j(t) \neq 1$ at the time of event e .

Lastly, note that interventional measures such as social distancing – sparsifying $P_{i,k}(t)$ – or business restrictions – reducing β_k – always *reduce* the original exposure rates $\lambda_{j \rightarrow i}^*(t)$ in Eq. 14, and can thus be implemented in a straightforward manner using thinning by rejecting affected exposure events with some probability.

E.4 Queue-based sampling algorithm

Combining our considerations above, we arrive at an efficient sampling procedure based on a single temporally-sorted priority queue Q for generating sound simulations of the model SDEs. The comprehensive algorithm is defined as Algorithm 1 and the sampling of exposure times explicitly described in Algorithm 2. For simplicity, we omit details about the procedure $\text{INTERVENTIONS}(i, j, k, t)$, which applies the above-mentioned thinning due to social distancing and business restrictions, and point the reader to our publicly available implementation for details [36].

F State variable initialization

While background exposures in *Scenario B* are straightforwardly modeled by adding a constant base rate $\lambda_{0,i}^*(t)$ to $\lambda_i^*(t)$ in the exposure counting processes $N_i(t)$ (e.g., modelling visits to neighboring regions), there need to be non-degenerate initial conditions when modeling *Scenario A* and for parameter estimation during the same period. Since COVID-19 case data is available during this time window, we decide to heuristically compute aggregate initial seed counts for the state variables using the observed cases as well as results from recent COVID-19 literature. The starting point of *Scenario A* is selected such that approximately five to ten COVID-19 cases occurred in a given region.

Specifically, we set the number of initially symptomatic individuals $I_{\text{init}}^s = \sum_{i \in \mathcal{V}} I^s(0)$ equal to the real observed COVID-19 cases in a region, or scaled proportionally to the population size within an administrative region, at the start date of simulation and assume that all have been positively tested. Based on the above, we initially seed $I_{\text{init}}^a = \alpha_a / (1 - \alpha_a) I_{\text{init}}^s$ individuals to be asymptomatic, to obtain a proportion of α_a initially asymptomatic seeds. The asymptomatic individuals has been recently estimated to account for roughly $\alpha_a = 0.4$ of the infected [22, 63, 64]. Lastly, assuming that infectious individuals have exposed R_0 others themselves on average, we initially seed $E_{\text{init}} = R_0 (I_{\text{init}}^a + I_{\text{init}}^s)$ exposed individuals, where we use recent estimates of the basic reproduction number of approximately $R_0 = 2.0$ [22, 65, 66].

At the beginning of a model simulation in *Scenario A*, the initially exposed, asymptomatic, and symptomatic are selected uniformly at random from the population based on the above heuristics, and neither asymptomatic nor symptomatic seeds cause further exposures in the model. No other states are seeded for simplicity. We note that the question of initialization can generally never be satisfactorily addressed when applying a model representing states not observed in reality.

G Mobility patterns

We set the value of the site visit intensities $\lambda_{i,k}(t)$ and v_k in our mobility model using the following demographic and geolocation data, which we also visualize in Figures 15 and 16 for all the considered towns and regions:

- **Demographic data:** We use publicly available high-resolution population density data provided by *Facebook Data for Good* [67]. For our experiments, the respective maps are split into equally-sized

tiles. The total population of the respective area is proportionally distributed across the available tiles according to the aggregate population density of each tile. We randomly distribute the individuals of each tile to six or nine age groups \mathcal{A} according to the real demographics of the region, matching the age groups of the COVID-19 case data collected by the national authorities in Germany and Switzerland, respectively [42, 43]. Ultimately, these individuals are placed in households of sizes one to five according to their age categories and the household structure in the respective country [51, 52].

- **Geolocation data:** We use publicly available geolocation data provided by OpenStreetMap, which contains the specific location of sites of many different categories in our regions of interest. Specifically, we retrieve the location of all sites \mathcal{S} within five site categories, while we would like to highlight that one could consider other types of sites available through the OpenStreetMap API [68].

- *Education*: Schools, universities, and research institutes
- *Social*: Restaurants, cafes, bars, and pubs
- *Transportation*: Bus stops
- *Work*: Offices and shops
- *Groceries*: Supermarkets and convenience stores

We assume that each individual $i \in \mathcal{V}$ in age group $a(i) \in \mathcal{A}$ visits only a constrained set of sites $\mathcal{S}_i \subseteq \mathcal{S}$. This reflects the fact that individuals typically study or work at only one place, form habits regarding the public transportation they use, and social places or supermarkets they visit. To construct \mathcal{S}_i , we sample u_c different sites from each site category c with probability inversely proportional to the distance from the individual’s home, where $u_c = 1$ for education, $u_c = 10$ for social, $u_c = 5$ for transportation, $u_c = 1$ for work, and $u_c = 2$ for groceries.

Moreover, for each individual i and site $k \in \mathcal{S}_i$, we set the intensity $\lambda_{i,k}(t) = r_{a(i),c(k)}/u_{c(k)}$, where $r_{a(i),c(k)}$ is a constant value that depends on the individual’s age group $a(i) \in \mathcal{A}$ and the site type $c(k)$, as shown in Table 4. Here, we assume people of younger ages spend most of their time in school and social sites, middle-age people spend most of their time at work and elderly people have lower activity over all. Finally, for each site $k \in \mathcal{S}$, we set the mean duration $1/v_k = 1/v_{c(k)}$ of any visit to the site heuristically according to the site type $c(k)$. Specifically, we set the mean visit duration at educational sites to 2 hours, at social sites to 1.5 hours, in public transportation to 12 minutes, at work to 2 hours, and at supermarkets to 30 minutes.

Note that the duration of visits to sites within the categories education and work are set to lower values than one would expect as real visit durations. This accounts for the fact that people are neither exposed to all others at the site nor continually exposed during the visit. For instance, an office worker mainly interacts with a specific subset other people during lunch or group meetings, and students mainly interact with other students of their class during breaks and study sessions. We emphasize that our epidemiological model is not constrained to this setting and could be arbitrarily generalized by practitioners if desired or replaced by real or more fine-grained mobility or tracing data when available.

H Experimental setup for parameter estimation

In this section, we provide additional details on the experimental setup used for parameter estimation via Bayesian optimization. A summary of the complete estimation procedure is given as Algorithm 3.

H.1 Optimized parameters

As pointed out previously in Section 3, any set of parameters θ can be optimized globally using Bayesian optimization (BO). However, to improve identifiability and avoid overfitting, we decided to estimate the transmission rates $\beta = \beta_k$ and ξ due to infectious individuals at the sites they visit and at their households, respectively, and the mobility reduction p due to social distancing.

For each of the cities and regions, we run our estimation procedure separately. One central challenge for parameter estimation using real COVID-19 case data is that the epidemic did not evolve without interventions.

Algorithm 3 Parameter estimation using Bayesian optimization

Input: Black-box simulator $\mathbf{g}(\theta)$, parameter domain $\text{dom}(\theta)$, time horizon T , case data $c_{1:T}^{\text{true}}$, hyperparameters N, M, J

- 1: $s(\mathbf{x}) := -\sum_{t=1}^T (c_t^{\text{true}} - \mathbf{x}_t)^2$
- 2: $\theta_{1:M} \leftarrow$ first M points of Sobol sequence in $|\theta|$ dimensions, scaled from unit cube to $\text{dom}(\theta)$
- 3: $\mathcal{D} \leftarrow \emptyset$
- 4: **for** $i \in [M]$ **do** ▷ Initial quasi-random exploration
- 5: Obtain noisy sim. evaluation $\mathbf{g}(\theta_i)$ from J random roll-outs
- 6: $\mathcal{D} \leftarrow \mathcal{D} \cup \{(\theta_i, \mathbf{g}(\theta_i))\}$
- 7: **while** $|\mathcal{D}| \leq N$ **do** ▷ Bayesian Optimization
- 8: $p(\mathbf{g}(\theta)) \mid \mathcal{D}) \leftarrow \text{GP}(\mathcal{D})$
- 9: $\theta^* \leftarrow \arg \max_{\theta \in \text{dom}(\theta)} \text{KG}(\theta)$
- 10: Obtain noisy sim. evaluation $\mathbf{g}(\theta^*)$ from J random roll-outs
- 11: $\mathcal{D} \leftarrow \mathcal{D} \cup \{(\theta^*, \mathbf{g}(\theta^*))\}$
- 12: **return** $\arg \max_{(\theta, \mathbf{g}(\theta)) \in \mathcal{D}} s(\mathbf{g}(\theta))$

More specifically, the spread of COVID-19 was significantly influenced by social distancing measures and business restrictions in both Germany and Switzerland during most of the time periods for which data is available. The period of most restrictive measures, also referred to as the “lockdown”, occurred largely from March 23, 2020 to May 3, 2020 in Germany, and from March 16, 2020 to May 10, 2020 in Switzerland [48–50]. To be able to make use of COVID-19 data from the entire time period described as *Scenario A*, we account for the restrictions in place during the “lockdown” by

- (i) scaling down β at sites of specific types to mimic *business restrictions* and *closures*. Specifically, we reduce the individual transmission rate at educational sites, workplaces and social sites by 50% during the period of the “lockdown”; and,
- (ii) letting individuals practice *social distancing* by skipping a given planned visit in the mobility model with probability p during the “lockdown”. This social distancing factor p controls how strictly governmental interventions were followed in a given town and guides how much the case curve flattened during the “lockdown”.

Here, note that before the “lockdown”, *i.e.*, in periods without intervention, p and the β -multipliers at sites are ignored by the model. Hence, we jointly estimate the three parameters $\theta = \{\beta, \xi, p\}$ over the time period that we denote as *Scenario A* for a given region, *i.e.*, for a period of approximately two months until the end of the strict “lockdown” in either country, where all three parameters can be deemed identifiable because the estimation windows spans periods both before and during times of interventional measures.

H.2 Bounds

Bayesian optimization globally maximizes a black-box function over a constrained domain. However, the domain $\text{dom}(\theta)$ of $\theta = \{\beta, \xi, p\}$ is unbounded, since intensities of counting processes are only required to be non-negative. Nonetheless, in practice we observe that large values of β and ξ lead to far worse simulated outcomes than observed in COVID-19 case data, hence being suboptimal. From prior experiments, we empirically decide to estimate the parameters β and ξ over the domain $[0, 1.5]$ in all regional models, while keeping $p \in [0, 1]$ as p is a probability. The maximization of the knowledge gradient acquisition function is done using the internal optimization procedures of BoTorch.

H.3 Hyperparameters

We choose to run $M = 20$ initial quasi-random settings and optimize θ for a total of $N = 100$ steps for the computationally less demanding cities, *i.e.*, Tübingen, Kaiserslautern, and Locarno, and for a total of $N = 40$ for the computationally more demanding city of Bern, the Canton of Jura, and the Landkreis of Rheingau-Taunus. Each evaluation of the objective for a given setting θ of our simulator was the mean of $J = 96$ random realizations of our model over the time period. As mentioned in Section 3, in addition to the

stochasticity inherent to the counting processes, the simulations were randomized across realizations of the mobility traces and the selected individual infection seeds.

H.4 Efficient parameter estimation using downscaled models

In our experiments, for each selected region, we simulate the state, mobility pattern, and contacts of every single individual in the true population. However, for parameter estimation via Bayesian optimization (BO), we downscale the models, *i.e.*, we downscale the population and sites by a factor K uniformly at random⁶, for efficiency reasons. In this way, we avoid inefficiently long wall times due to worse-than-observed courses of the epidemic. Refer to Table 5 for details on the downscaling factor K used in each town and region.

I Parameter estimation using downscaled models might fail

As discussed in section H, to boost efficiency, we perform parameter estimation using downscaled models. In this section, we discuss potential issues one might face when employing downscaled models.

While we have found that using downscaled models for parameter estimation works well in most practical scenarios, there do exist settings where it can fail. More specifically, the full-scale model may not provide accurate predictions under the estimated parameters $\{\beta, \xi, p\}$ found using the downscaled model. In the remainder, we analyze one of these settings, the Landkreis of Tirschenreuth in Germany, a rural region with a high level of infections as of today, as shown in Figure 17. Landkreis Tirschenreuth shows specific properties that distinguish the area from the other cities and regions we analyzed, which can reveal why parameter estimation using a downscaled model might fail in some cases.

With a case incidence of 1,575 cases per 100,000 inhabitants as of July 13, 2020 [42], the region is more affected than the other cities and regions we considered. As a result, 7.69% of the population needs to get positively tested in order to match the COVID-19 case data under the *downscaled* model. Considering that the number of infected individuals might be much higher, this can lead to a significant decrease in the relative number of susceptible people due to large proportions of the population being either infected or recovered. For the epidemic to reach the target case incidence, parameter estimation will have to find larger transmission rates β_k to overcome the resulting reduction in infections. In contrast, under the full-scale model, only 1.54% of the population would have to get positively tested to match the COVID-19 case data, suggesting that the reduction in the number of susceptible individuals will have a smaller impact. As a consequence, in Landkreis Tirschenreuth, the predictions under the full size model are too pessimistic, as shown in Figure 17.

On top of that, sites are clustered into a number of villages, as shown in Figure 18a, which is a major distinguishing factor of Landkreis Tirschenreuth compared to other regions with high infection levels. In the second most heavily affected area, Tübingen, only 5.42% of the population need to get positively tested to match the COVID-19 case data under the downscaled model, and the city shows no local clusters in the population density and site distribution; see Figure 15. As a consequence, removing a large proportion of sites at random, as shown in Figure 18b, may change the properties of the mobility patterns under the downscaled model and lead to local and isolated infection herds in which potentially large proportions of the population are getting infected, further exacerbating the above observations.

When estimating the mobility-related model parameters using downscaled models, we recommend choosing a conservative scaling factor, such that mobility patterns remain qualitatively similar, and infection levels continue to be low enough to expect equal exposure dynamics at both scales.

J Narrowcasting the empirical probability of exposure

As recently noted by Chan et al. [57], health authorities may like to use contact tracing data of individuals who have been tested positive to *narrowcast* messages to the population, *i.e.*, make public service announcements that are highly tailored to a location or to a subset of individuals who have been in a certain location during

⁶Note that we do not downscale the initial state variable seeds and the COVID-19 case counts.

a specific period of time. For example, health authorities may like to inform the population about the risk of infection for individuals who visited a specific site in a certain period of time. While some individuals may be reluctant to adopt contact tracing technology due to privacy concerns, they may still be willing to follow public service announcements regarding quarantine or testing. For example, an individual may be willing to self-isolate or seek testing if they learn via narrowcasting that they recently visited a location with empirically high probability of exposure by other infected individuals.

To implement narrowcasting of exposure risk at sites \mathcal{S} , our model allows for the estimation of the empirical probability of exposure $\hat{p}_k([t_0, t_f])$ of an individual during a time window $[t_0, t_f]$, caused by positively tested individuals i that visited site k , i.e.,

$$\hat{p}_k([t_0, t_f]) \propto 1 - \prod_{\substack{i \in \mathcal{S} \\ T_i^+(t_0)=1}} \exp \left(- \int_{t_0}^{t_f} \int_{t'-\delta}^{t'} P_{i,k}(\tau) e^{-\gamma(t'-\tau)} d\tau dt' \right) \quad (15)$$

Perhaps surprisingly, the above computation does not suffer from the “ x^2 adoption problem” of contact tracing [22, 38] because it only requires $P_{i,k}(t)$ of positively tested individuals i , rather than both $P_{i,k}(t)$ and $P_{j,k}(t)$. For the same reason, it also requires data from location-based contact tracing systems where $P_{i,k}(t)$ is observed. However, in principle, one could also resort to proximity-based tracing systems if Bluetooth beacons are in place, as noted by Langford [38].

Figure 19 presents an example of narrowcasting of site-specific exposure probabilities during *Scenario A* with the estimated “lockdown” measures. Here, note that, as long as the level of adoption is uniformly distributed across visitors, the site ranking by exposure probability will be invariant to adoption levels in expectation. In this case, the absolute value of the probability of exposure can be corrected for the level of adoption. In practice, it would be important to correct for compliance disparities across sites and site types, which are likely to occur due to differences in demographics and visiting patterns at certain sites.

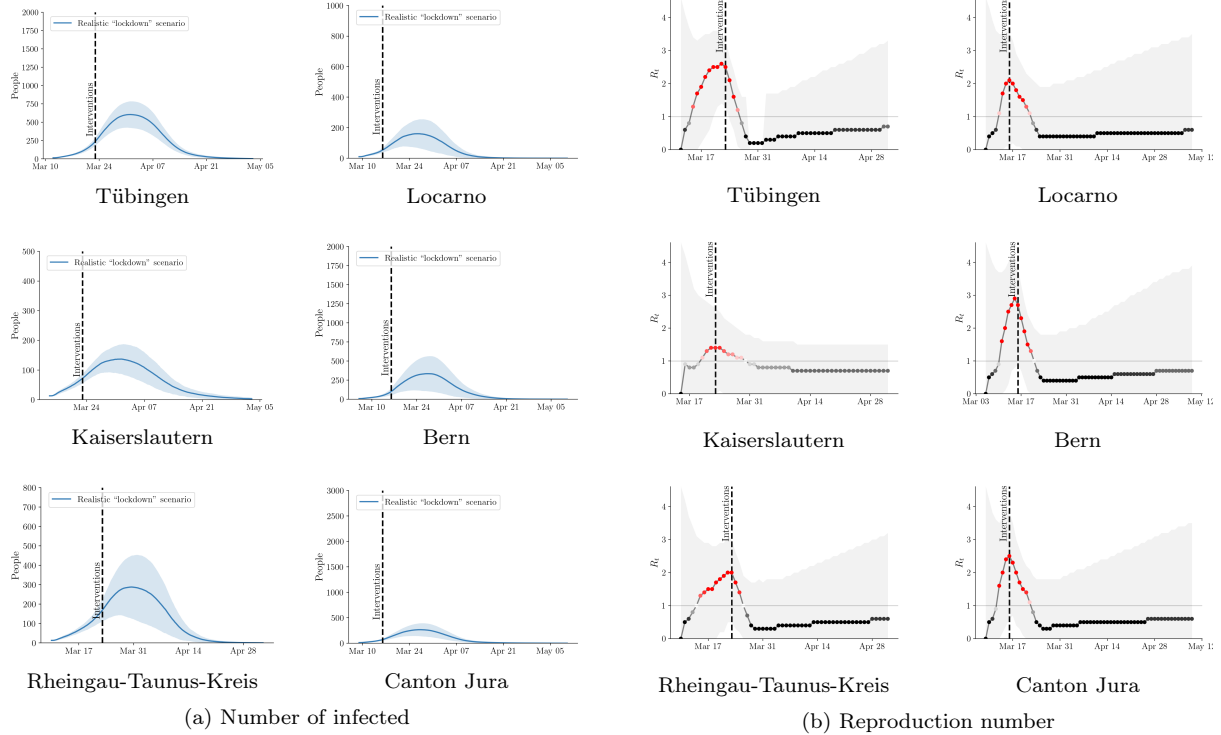


Figure 8: **Number of infected and effective reproduction number in the realistic scenario.** Panel (a) shows the number of infected in the realistic scenario used for parameter estimation with the “lockdown” interventions described in Appendix H. The line represents the mean of the number of infected over 48 random realizations of the simulations, the shaded regions correspond to two times the standard deviation. Panel (b) shows the corresponding effective reproduction number computed using the Bayesian approach in Bettencourt et al. [69, 70], the line represents the most likely estimate and shading represents high density areas.

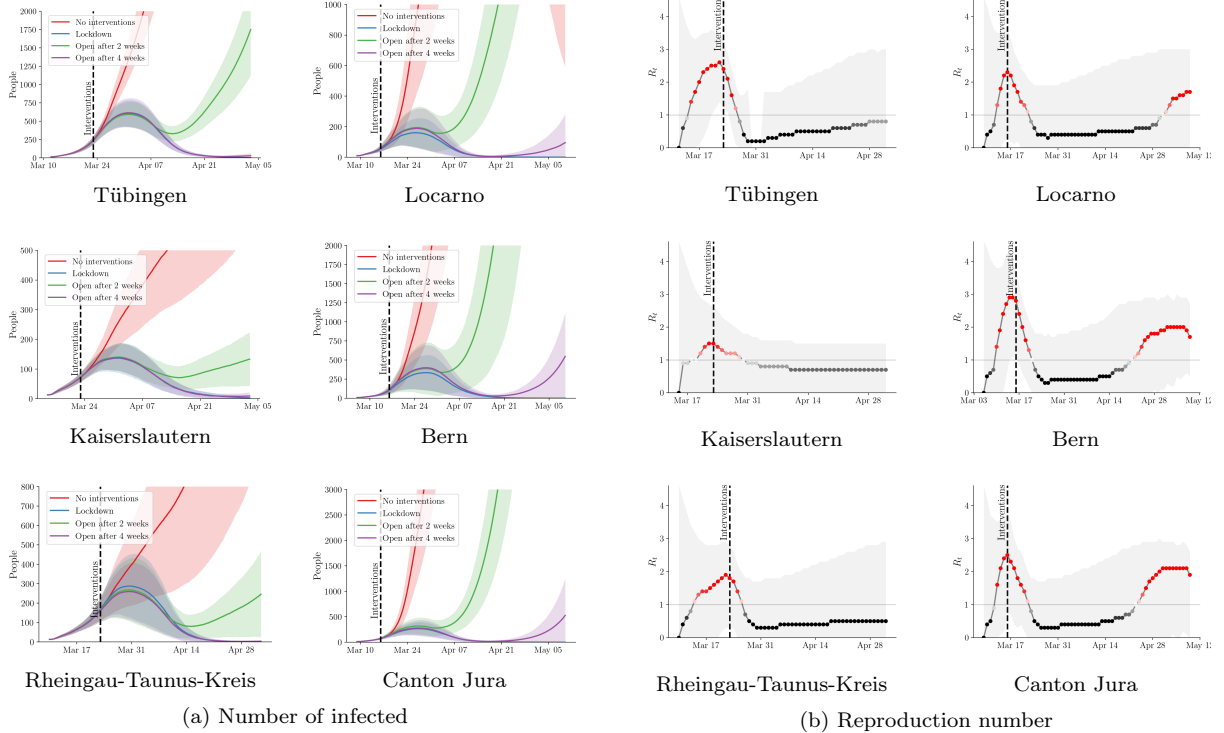


Figure 9: **Early ending “lockdown”.** Counterfactual what-if scenario in which the same restrictive measures that were in place during the “lockdown” period are implemented for shorter time periods. The lines in panel (a) represent the mean of the number of infected over 48 random realizations of the simulations, the shaded regions correspond to two times the standard deviation. Panel (b) shows the effective reproduction number within the scenario of the 4-weeks “lockdown” corresponding to the purple line in panel (a). The line represents the most likely estimate and shading represents high density areas.

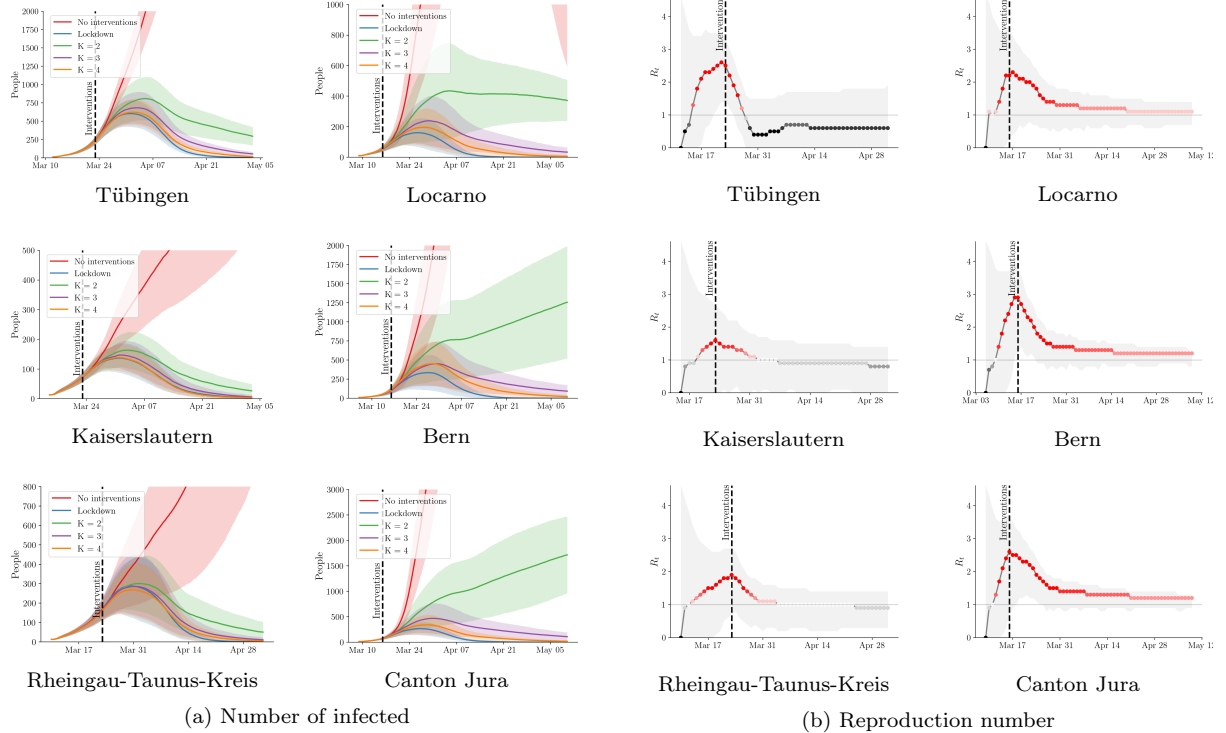


Figure 10: **Alternating curfews.** Counterfactual what-if scenario in which the population is divided into K groups and, on each day, only one group is allowed to follow their usual daily activities. Panel (a) shows the daily number of infected for different numbers of groups. The lines represent the mean of the number of infected over 48 random realizations of the simulations, the shaded regions correspond to two times the standard deviation. Panel (b) shows the effective reproduction number for the scenario of $K = 2$ groups. The line represents the most likely estimate and shading represents high density areas.

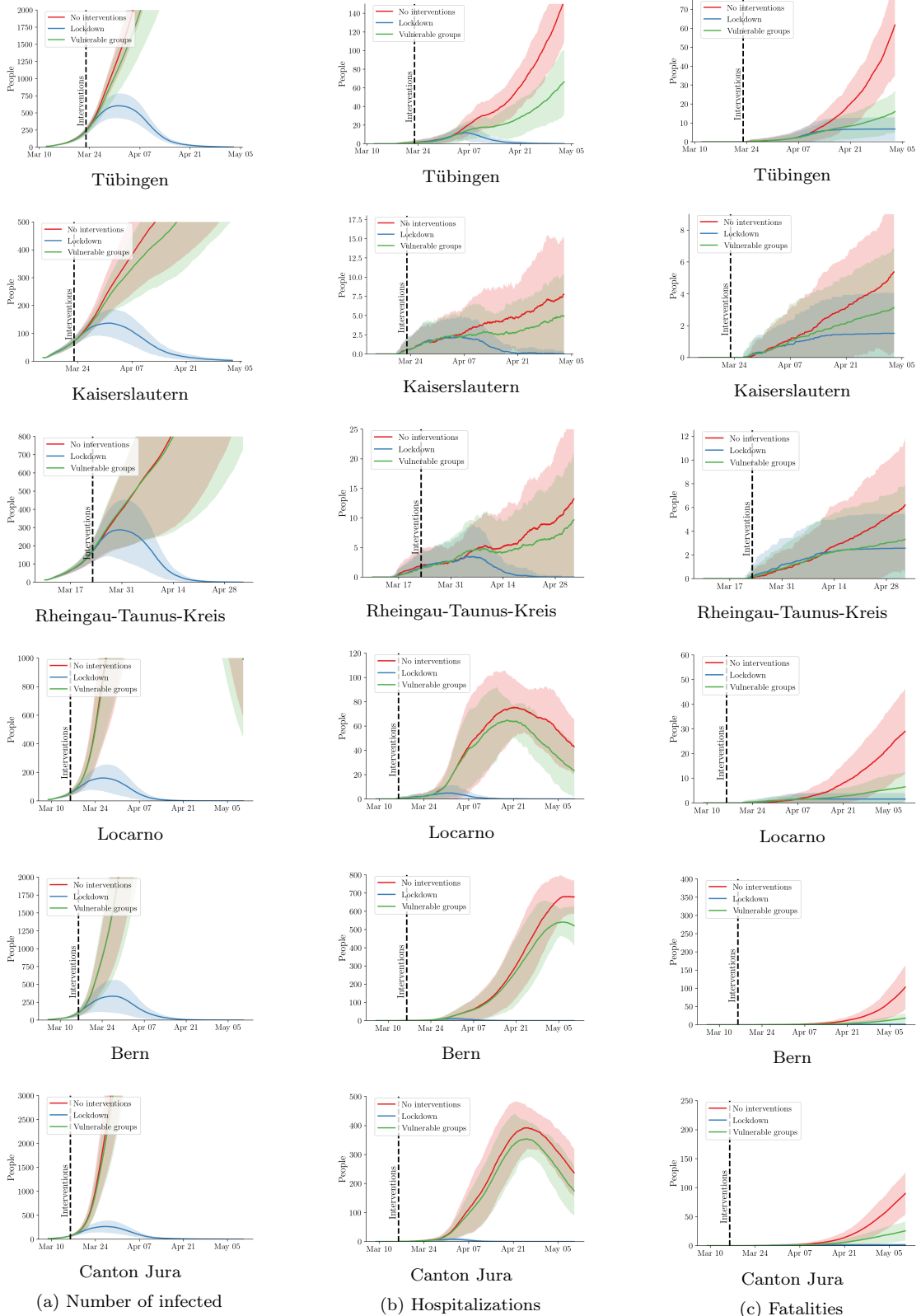


Figure 11: **Social distancing of vulnerable groups.** Counterfactual what-if scenario in which the same social distancing measures as in the “lockdown” scenario are imposed only on vulnerable groups. Panel (a) shows the daily number of infected, panel (b) and (c) the hospitalizations and fatalities, respectively. The lines represent the mean over 48 random realizations of the simulations, the shaded regions correspond to two times the standard deviation.

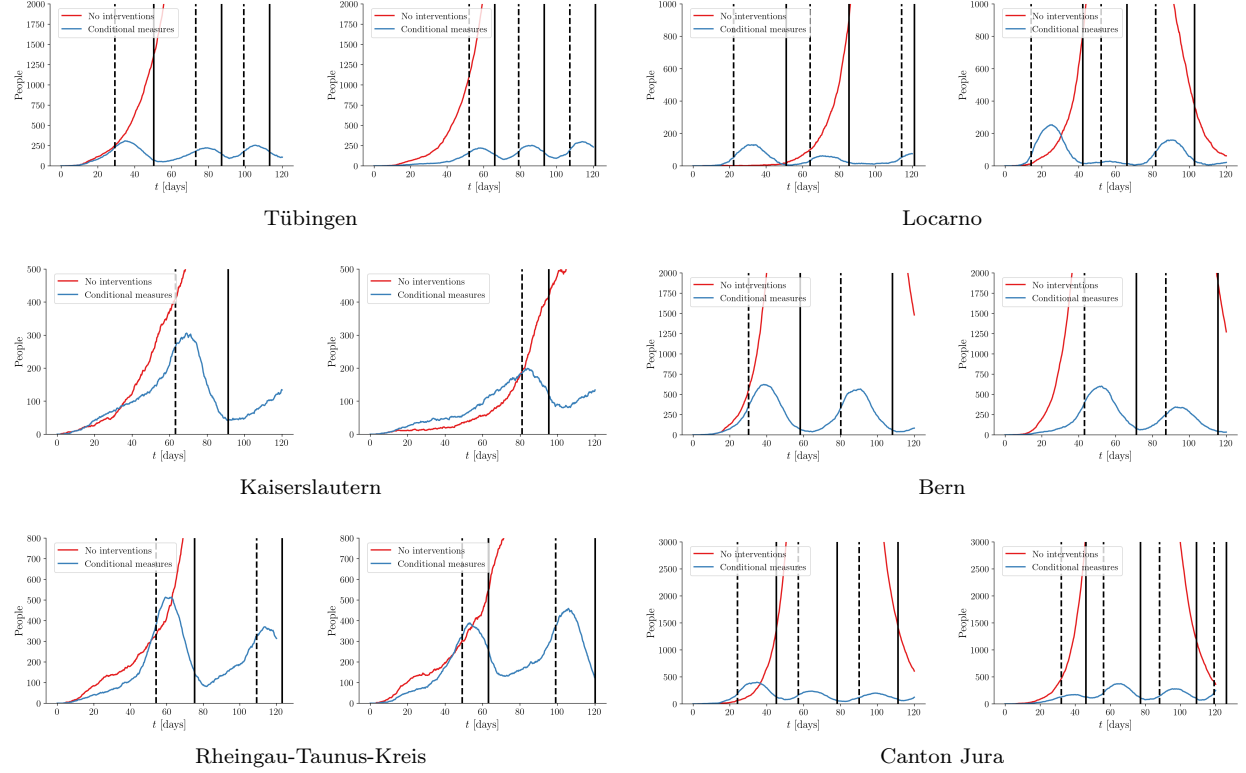


Figure 12: **Conditional “lockdowns” based on weekly incidence.** The panels show the number of infected people for two single realizations of the simulation of *Scenario B*. Whenever the number of positive cases within 7 days exceeds the threshold of 50 per 100,000 inhabitants, we implement the same restrictive measures that were in place during the “lockdown” period in *Scenario A*. Dashed and solid vertical lines indicate beginning and ending of the conditional “lockdowns”, respectively.

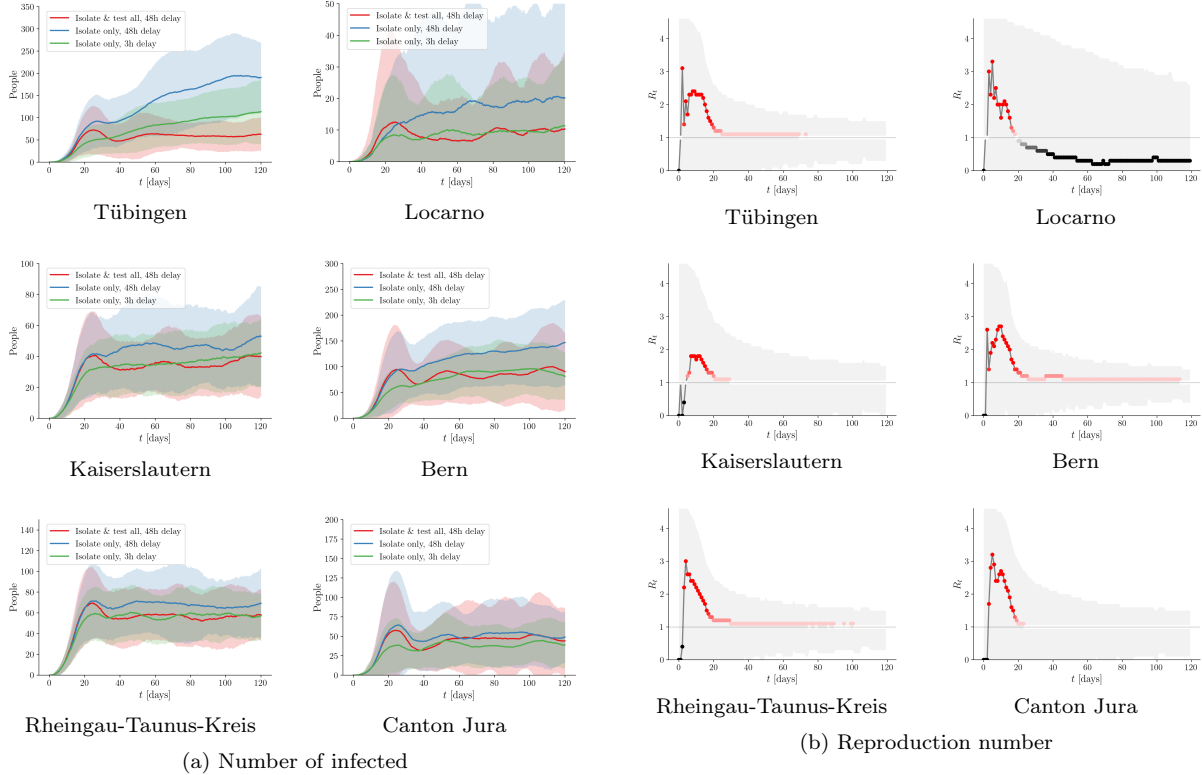


Figure 13: **Contact tracing strategies.** Numbers of infected for various contact tracing strategies in *Scenario B*. Panel (a) shows the efficacy of tracing strategies under full compliance when identified contacts are isolated and/or tested with different reporting delays. Lines and shading indicate the mean and two times the standard deviations over 48 random roll-outs. Panel (b) shows the effective reproduction number for the tracing strategy with isolating and testing all contacts with 48 hours test delay under full compliance. The line represents the most likely estimate and shading represents high density areas.

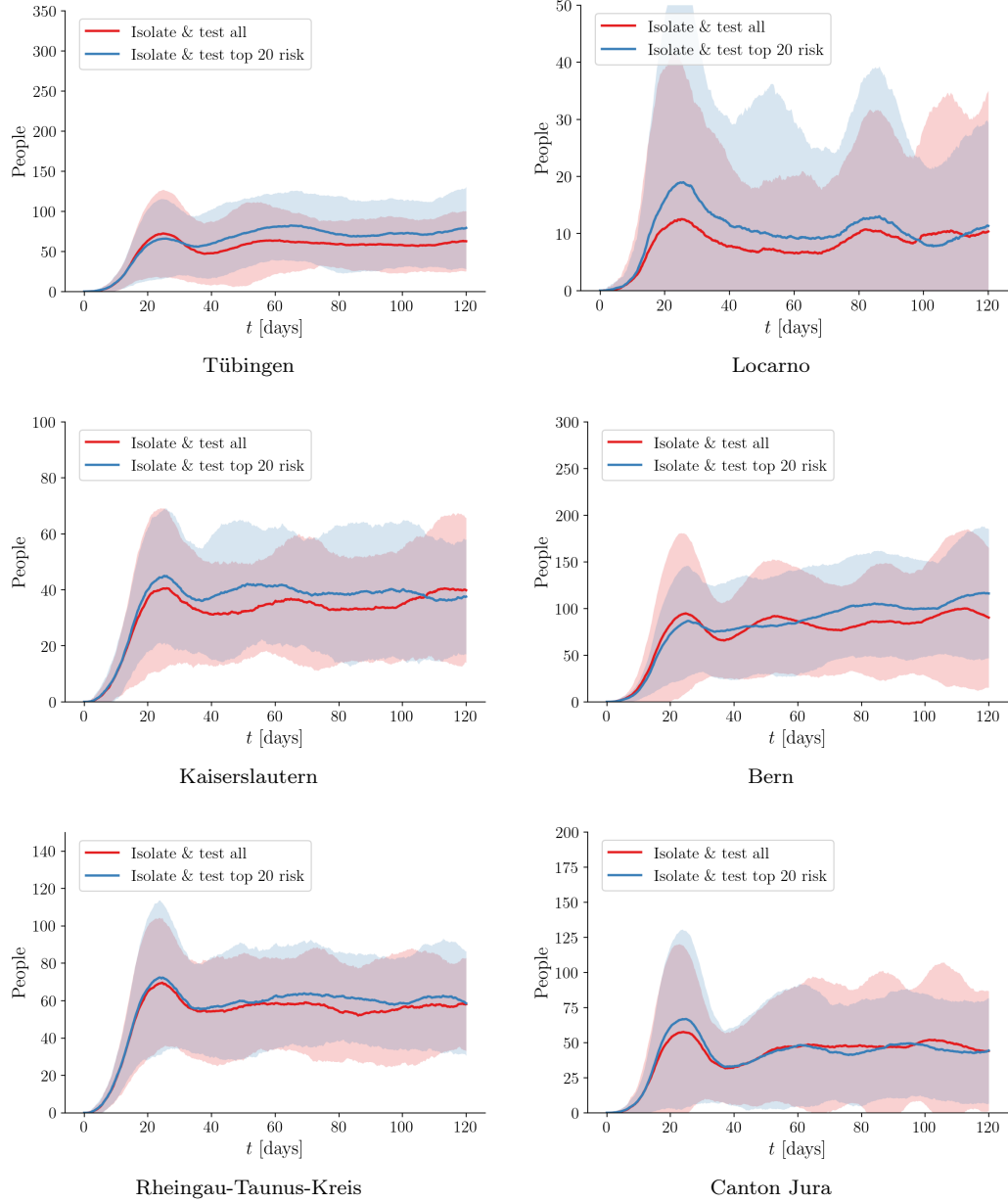
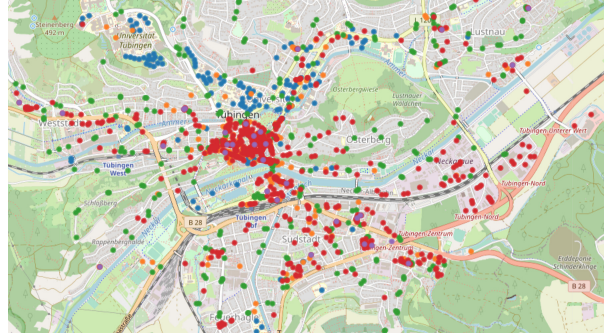


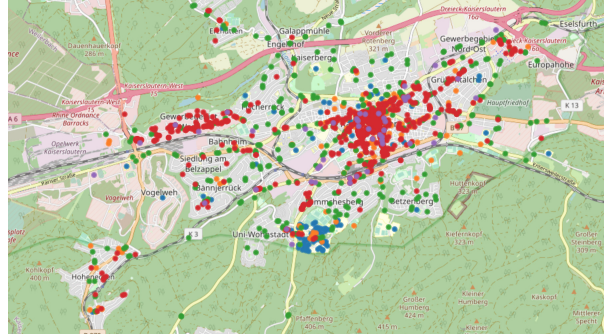
Figure 14: **Advanced testing strategy.** Number of infected in *Scenario B* under the two contact tracing strategies of isolating and testing all contacts of a positively tested individual with 48 hours test delay and only testing the 20 contacts with the highest empirical infection probability. Lines and shading indicate the mean and two times the standard deviations over 48 random initializations. The strategy of testing only 20 contacts reduces the number of conducted tests by 70-90%.



(a) Site locations in the mobility model of Tübingen



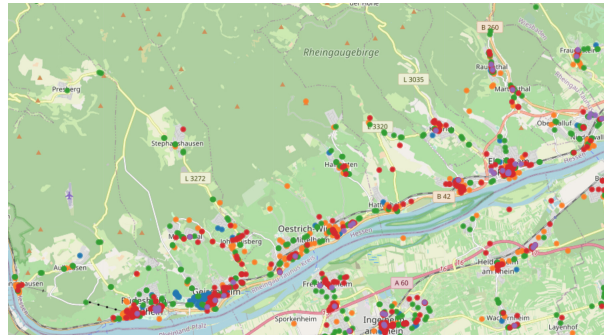
(b) Population density in the mobility model of Tübingen



(c) Site locations in the mobility model of Kaiserslautern



(d) Population density in the mobility model of Kaiserslautern

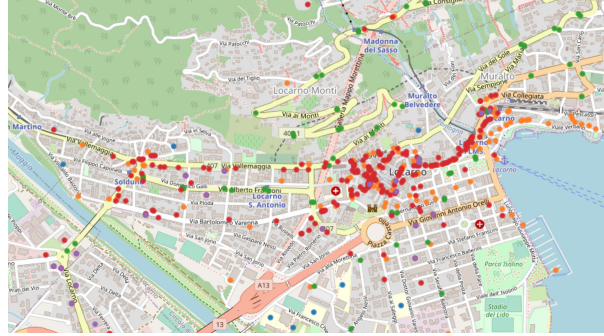


(e) Site locations in the mobility model of Rheingau-Taunus-Kreis

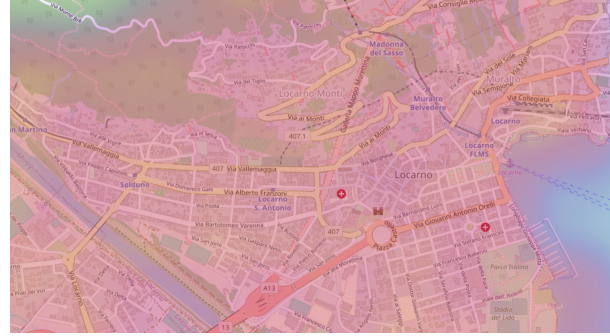


(f) Population density in the mobility model of Rheingau-Taunus-Kreis

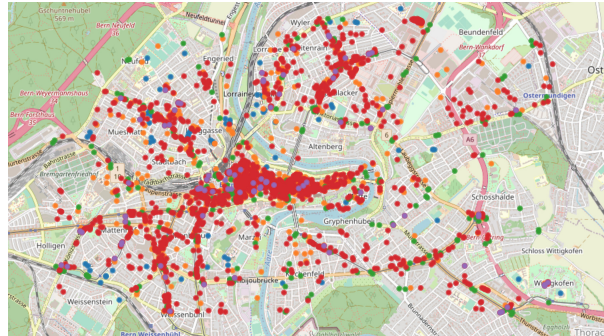
Figure 15: Spatial distribution of site locations and population density in the mobility models of Tübingen, Kaiserslautern, and the Landkreis of Rheingau-Taunus, Germany. In the left column, circles depict schools, universities and research institutes (blue), social places (orange), bus stops (green), workplaces (red), and supermarkets (purple). In the right column, purple and orange colors correspond to low and high population density areas, respectively.



(a) Site locations in the mobility model of Locarno



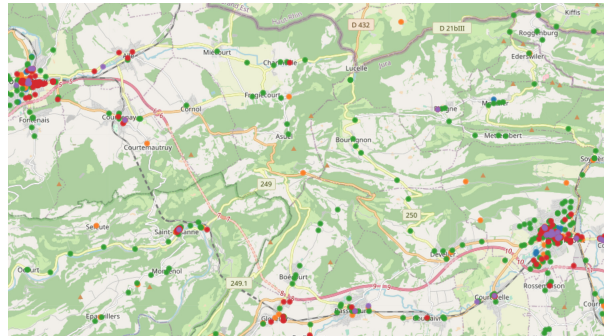
(b) Population density in the mobility model of Locarno



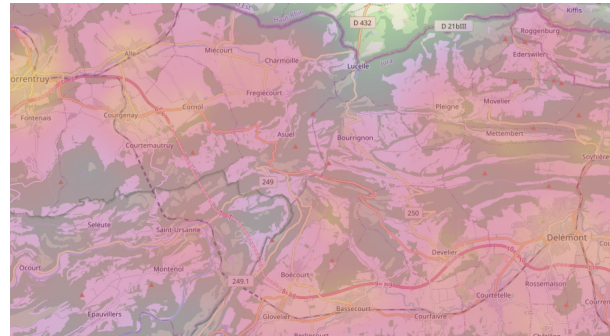
(c) Site locations in the mobility model of Bern



(d) Population density in the mobility model of Bern



(e) Site locations in the mobility model of Canton Jura



(f) Population density in the mobility model of Canton Jura

Figure 16: **Spatial distribution of site locations and population density in the mobility models of Locarno, Bern and the Canton of Jura, Switzerland.** The colors depict the same categories and densities as in Figure 15.

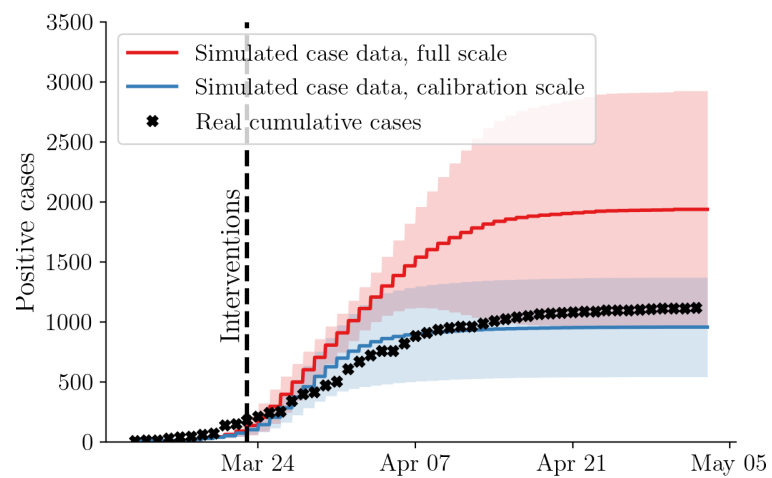
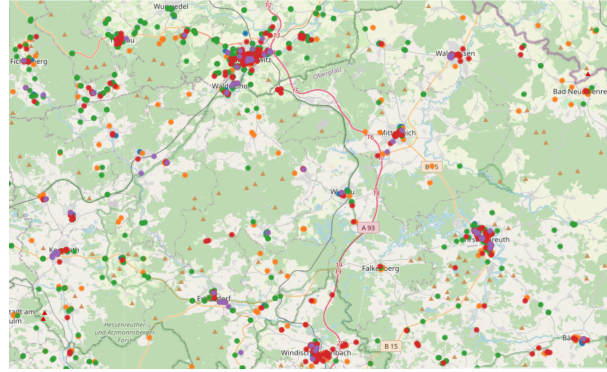
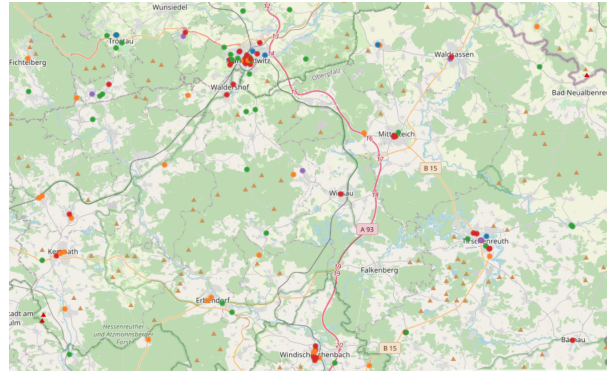


Figure 17: **Cumulative number of positively tested individuals for Landkreis Tirschenreuth, Germany.** The blue line corresponds to the calibration scenario in which the population and the sites are scaled down by a factor of ten. The red line corresponds to the full scale simulation. Line and shading indicate mean and two times the standard deviation over 48 random initialization.



(a) Site locations, full scale



(b) Site locations, downsampled



(c) Population density

Figure 18: Site locations and population density in Tirschenreuth, Germany. Panel (a) corresponds to the spatial site distribution of the full scale version, while panel (b) shows a downsampled version in which the number of sites is reduced by a factor of ten. Colors represent site types as defined in Figure 15. Panel (c) shows the population density taken from *Facebook Data for Good* [67]. Purple and orange colors correspond to relative low and high density of homes in the region, respectively.

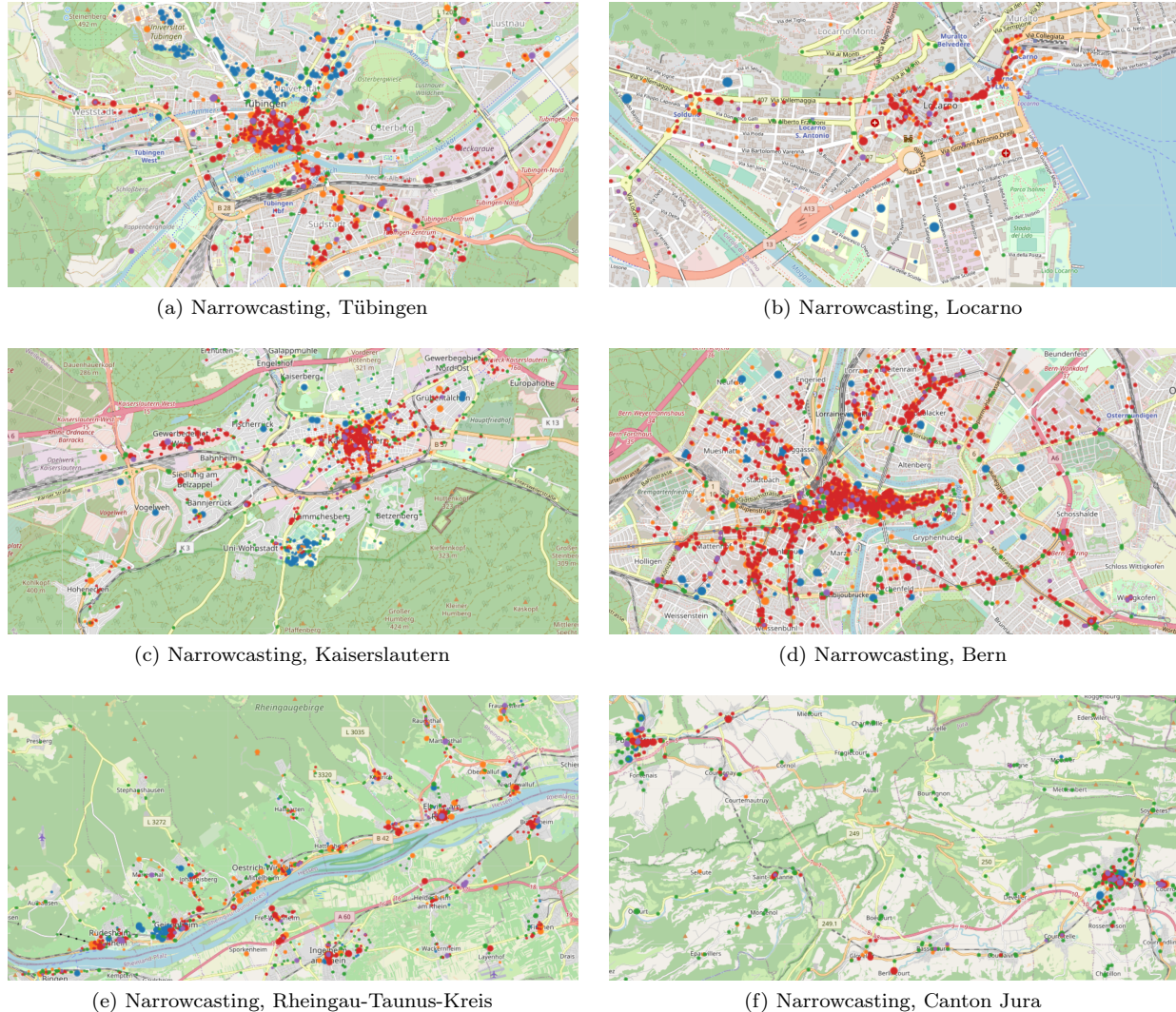


Figure 19: **Narrowcasting of exposure probabilities at sites during a week-long window of the observed lockdown scenario of Figure 8.** Circles represent sites and the size of each circle is proportional to the site's empirical probability of exposure of a visiting individual during the time period of two weeks. Colors represent site types as defined in Figures 15 and 16.

Table 2: Epidemiological distributions and model parameters in units of days. The hospitalization and fatality rates α_h and α_b mentioned in the main paper are estimated from COVID-19 case data in a studied region and is age-dependent. Log-normal parameters indicate the mean and standard deviation of the underlying normal distribution.

Counting process	Starts when	$\log \mathcal{N}$ parameters	Source
$M_i(t)$	$dE_i(t) = 1$	$(0.9470, 0.6669)^{\ddagger}$	[60]
$R_i^s(t), R_i^a(t)$	$dI_i^s(t) = 1$	$(2.6365, 0.0713)^{\ddagger}$	[66, 71, 72]
$W_i(t)$	$dI_i^p(t) = 1$	$(0.7463, 0.4161)^{\ddagger}$	[71]
$Y_i(t)$	$dI_i^s(t) = 1$	$(1.9358, 0.1421)^{\ddagger}$	[73]
$Z_i(t)$	$dI_i^s(t) = 1$	$(2.5620, 0.0768)^{\ddagger}$	[61]
Parameter	Value	Description	Source
α_a	0.4	proportion of asymptomatic individuals	[22, 63, 64]
μ	0.55	relative asymptomatic transmission rate	[25]
γ	$0.3465 h^{-1}$	decay of infectiousness at sites	[37]
δ	$4.6438 h$	window of non-contact contamination¶	[37]

‡ Incubation period from [60], here corrected not to encompass the estimated time of pre-symptomatic infectiousness [71].

§ Approximate log-normal parameters constructed because COVID-19 literature results only reported using mean or median estimates of times.

¶ For computational purposes, set from γ by the time when rate of infection drops below 20% after leaving a site.

Table 3: Summary of towns and regions studied in Germany and Switzerland. *(Land)Kreis* denotes the district-level, *Kanton* the state-level administrative unit in Germany and Switzerland, respectively. *Incidence* denotes the number of COVID-19 cases per 100,000 inhabitants registered before July 13, 2020 and was taken at *Landkreis* and *Kanton*-level from data provided by the national authorities [42, 43].

Region	Country	Population	Incidence	Severe?	Urban?
Rheingau-Taunus-Kreis	GER	187,157	144.8	-	-
Kanton Jura	CH	73,419	355.5	-	-
Kaiserslautern	GER	99,845	200.7	-	✓
Bern	CH	133,883	191.4	-	✓
Locarno	CH	15,826	943.8	✓	-
Tübingen	GER	90,546	570.1	✓	✓

Table 4: Average number $r_{a(i),c(k)}$ of visits per week to sites of type $c(k)$ by individuals of age group $a(i) \in \mathcal{A}$. The splits into age groups reflect the COVID-19 case data in Germany [42] and was extended equivalently to models in Switzerland with slightly more age groups [43].

Age Group $a(i)$	Education	Social	Transportation	Work	Groceries
0-4	5	1	-	-	-
5-14	5	2	3	-	-
15-34	2	2	3	3	1
35-59	-	2	1	5	1
60-79	-	3	2	-	1
80+	-	2	1	-	1

Table 5: Start and end dates in the year 2020 together with downscaling factors K used for model calibration in the case study. Start dates are chosen such that a given region had approximately five to ten confirmed COVID-19 cases, allowing for non-degenerate and comparable initial conditions.

Region	Country	K	Start calibration	Start lockdown	End calibration
Rheingau-Taunus-Kreis	GER	10	March 10	March 23	May 3
Kanton Jura	CH	10	March 9	March 16	May 10
Kaiserslautern	GER	10	March 15	March 23	May 3
Bern	CH	10	March 6	March 16	May 10
Locarno	CH	2	March 9	March 16	May 10
Tübingen	GER	10	March 12	March 23	May 3

Table 6: Parameter values found in model calibration separately for each selected region. Recall that β denotes the individual transmission rate at public sites, ξ the individual transmission rate in households, and p the social distancing factor, only active during the lockdown period listed in Table 5.

Region	Country	β	ξ	p
Rheingau-Taunus-Kreis	GER	0.1875	0.9375	0.8750
Kanton Jura	CH	0.1406	0.7031	0.8438
Kaiserslautern	GER	0.3004	0.4548	0.6327
Bern	CH	0.4688	0.2812	0.9375
Locarno	CH	0.7607	0.5394	0.9181
Tübingen	GER	0.7450	1.0842	0.8116

Table 7: Proportions of the population that have been positively tested until the end of the lockdown period according to the COVID-19 case data provided by the public health authorities. The right column shows the corresponding proportion in the downscaled simulation.

Region	Country	Downscaling	% pos. tested, full scale	% pos. tested, downscaled
Rheingau-Taunus-Kreis	GER	10	0.106	1.063
Kanton Jura	CH	10	0.279	2.792
Kaiserslautern	GER	10	0.124	1.240
Bern	CH	10	0.176	1.756
Locarno	CH	2	0.916	1.833
Tübingen	GER	10	0.542	5.423
Tirschenreuth	GER	5	1.537	7.685